THESIS FOR THE DEGREE OF DOCTOR OF PHILOSOPHY

Self Oscillations and Cooling of Carbon Based NEMS Devices

ANDERS NORDENFELT

GÖTEBORGS UNIVERSITET

Department of Physics
University of Gothenburg
SE-412 96 Göteborg, Sweden 2012

Self Oscillations and Cooling of Carbon Based NEMS Devices
ANDERS NORDENFELT
ISBN: 978-91-628-8460-4

Doktorsavhandling vid Göteborgs Universitet

Condensed Matter Theory
Department of Physics
University of Gothenburg
SE-412 96 Göteborg
Sweden
Telephone +46 (0)31 772 1000

Typeset in LaTeX

Figures created using K-Paint, MATLAB and Mathematica.

Printed by Aidla Trading AB
Göteborg, Sweden 2012

Self Oscillations and Cooling of Carbon Based NEMS Devices

ANDERS NORDENFELT
Condensed Matter Theory
Department of Physics
University of Gothenburg

ABSTRACT

We investigate the electromechanical properties of a number of system geometries featuring a doubly clamped Carbon Nanotube or Graphene sheet with a deflection sensitive resistance and an electronic feedback in the form of a Lorentz force or an electrostatic attraction. The nanotube is subjected to a constant current- or voltage bias and it is shown that when the electromechanical coupling exceeds a certain critical value the system becomes unstable to self-excitations of the mechanical vibrations accompanied by oscillations in the voltage drop and current through the nanotube. The critical value typically depends on the quality factor and some function of the mechanical and electronic relaxation times. We discuss applications of the devices as active tunable radiofrequency oscillators and for cooling.

Keywords: Nanoelectromechanical systems, NEMS, carbon nanotubes, suspended carbon nanotubes, self oscillations, negative differential resistance, oscillator, transmission line, cooling.

Research publications

This thesis, except Chapter 8, is an introduction to and summary of the following research articles.

PAPER I

Magnetomotive Instability and Generation of Mechanical Vibrations in Suspended Semiconducting Carbon Nanotubes
A. Nordenfelt, Y. Tarakanov, L. Y. Gorelik, R. I. Shekhter, M. Jonson
New Journal of Physics, 12, 123013, (2010)

PAPER II

Magnetomotive Cooling and Excitation of Carbon Nanotube Oscillations under Voltage Bias
A. Nordenfelt
Central European Journal of Physics, 9, 1288-1293, (2011)

PAPER III

Spin-controlled nanomechanics induced by single-electron tunneling
D. Radic, A. Nordenfelt, A.M. Kadigrobov, R. I. Shekhter, M. Jonson,
L. Y. Gorelik
Physical Review Letters, 175, (2011)

PAPER IV

Selective self-excitation of higher vibrational modes of graphene nano-ribbons and carbon nanotubes through magnetomotive instability
A. Nordenfelt
Accepted for publication in:
Journal of Computational and Nonlinear Dynamics

TABLE OF CONTENTS

Preface

Min bok är färdig - ack, hvad jag är glad -
Hvad fägring till format och yta!
Må allmänheten ej min auktorsfröjd förtryta!
Hvad nytta i hvartenda blad!
Hvad harm för herrar recensenter,
Magistrar och journalskribenter -
De finna icke här i någon enda rad
Ett ämne för den lärda möda,
De sig så oförtrutet ge,
Att hvarje bokligt foster döda,
Så snart det hunnit ljuset se.
Men re'n från denna tropp jag hör en hotelse:
»Ditt fräcka sjelfberöm, skribler, din dom förvärrar!»
O, nej, så måtte dock ej ske!
Det verk, jag vill i dagen te,
Det är - en nålbok, mine herrar!

'Boken'
av Anna Maria Lenngren

There are some people who have been particularly important for the process leading to results presented in this thesis. First and foremost my supervisor Leonid Gorelik who made the initial sketches for most of the device geometries considered and who introduced me to several of the analytical techniques that led to many important insights. Secondly, Anatoly Kadigrobov, who I believe at a certain moment led the work onto the path it later followed. Thirdly, Yury Tarakanov who was indespensible for the formation of Paper I and Danko Radic who was the lead author of Paper III. Finally, my examiner Mats Jonson who has perfomed a most rigorous proof-reading of nearly all my output and Robert Shekhter thanks to whom I am here in the first place and who also contributed to the before mentioned papers.

My gratitude also goes to Gustav Sonne who helped me with every kind of computer related issue, as well as to Milton, Giuseppe and Fabio for Italian lessons among other things, and to all the rest of the people at the Condensed Matter Theory group for stimulating scientific discussions and a nice working atmosphere.

CHAPTER 1

Introduction

In recent years much progress has been made in the development and fabrication of high performance nano electromechanical devices. The material that has boosted this rapid development, and which has been the focus of interest of the nano-physics community for almost a decade, is the two-dimensional carbon compund Graphene [1] and its close relative, the Carbon Nanotube (CNT) [2]. Apart from their excellent electronic performance, these materials posess mechanical properties that opens up for completely novel applications. High resonance frequencies combined with very low mechnical dissipation makes it possible to couple the electronic and mechanical degrees of freedom in ways that are unprecedented.

As part of this enterprise, extensive research has been aimed at examining how the electronic transport properties of carbon nanotubes and graphene are affected by mechanical deflection and a number of mechanisms that contribute to this change of conductance have been identified and quantified. The main purpose of the work presented in this thesis has been to explore and classify different ways to obtain electromechanical instability with resulting self-oscillations of suspended Carbon Nanotubes with such a displacement sensitive resistance. The active feedback mechanism that gives rise to the instability is typically a magnetically induced Lorentz force or an electrostatic attraction.

Most of the CNT-based devices that have been considered in the litterature are passive resonators that perform filtering of incoming radio-frequency signals. The bulk of the material presented here, however, points to another area of applications, namely the possibility to construct active tunable CNT-based oscillator devices that transform an incoming dc-signal to an ac-signal. To date, most of the active oscillators that have been realized in experiments rely on distance dependent field emission of electrons from a singly-clamped CNT to an electrode, see for example [3–5]. Another approach, which was proposed theoretically in the paper [6], relies on distance dependent electron injection from an STM tip into a doubly-clamped CNT. The advantage with some of the schemes proposed in this thesis is that, if succesfully implemented, they wouldn't require as precise geometry controle as its predecessors. Moreover, they are readily applicable to any device geometry that gives rise to a deflection sensitive resistance.

The story doesn't end there though. One of the side results obtained is that most of the schemes can be reversed so that instead of producing self-oscillations they cool down the spontaneus motion of the nanowire, see Chapter 6. Furthermore, in Chapter 7 we demonstrate that by increasing the complexity of the systems slightly there emerges a possibility to selectively excite harmonics above a certain frequency cut-off. In Chapter 8 the transmission line is analyzed within the same framework, and finally in Chapter 9 there is an analysis of a system in which the magnetic field plays a threefold role giving rise to a phenomenon which we chose to call 'Spintromechanics'.

CHAPTER 2

Elementary Properties of Carbon Nanotubes and Graphene

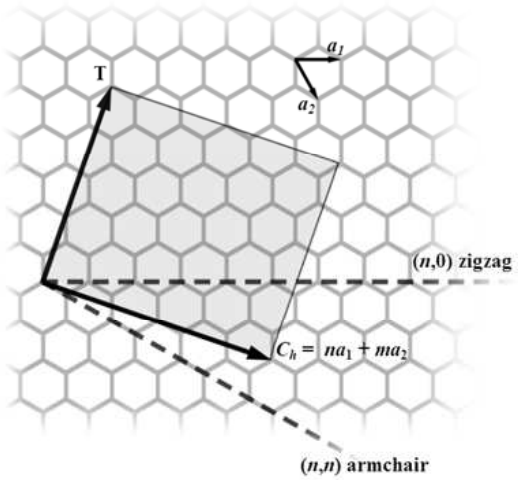

Figure 2.1: Lattice structure of graphene with the chiral vectors of armchair- and zigzag carbon nanotubes marked with dashed lines in the figure.

The study of carbon nanotubes and graphene nano-ribbons belongs to a sub-discipline of condensed matter physics commonly referred to as Mesoscopic Physics. This sub-discipline deals with objects whose spacial dimensions are on both the macroscopic and atomic scale, and thus exhibit some quantum behaviour that would not be present on the larger scale but at the same time allow some of its properties to be modelled by classical equations. Carbon nanotubes and graphene fit into this picture since its mechanical motion can often be succesfully modelled by continuum mechanics whereas the electronic transport properties may be fundamentally altered by small changes in their composition. As the same suggests, the radius of the nanotube is typically a few nanometers whilst the length may be considerably longer, the current world record beeing a few centimeters. Carbon Nanotubes can be thought of as a sheet of graphene that has been wrapped into a tube. Although they are not produced in this manner the picture nevertheless serves as a convenient means of classifying different types of carbon nanotubes. Graphene is a

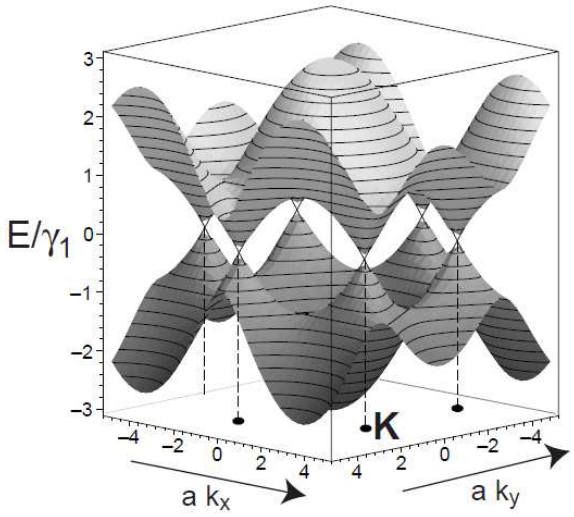

Figure 2.2: Graph of the dispersion relation for graphene given by equation 2.1.

carbon compund with a two-dimensional hexagonal structure which is usually represented by two lattice vectors $\vec{a}_1$ and $\vec{a}_2$ as shown in figure (2.1). A tube can be formed by wrapping the sheet joining two atoms separated by a vector which is an integer linear combination of the lattice vectors. This vector is called the chiral vector and its representation (m, n) in the lattice basis defines the so called chirality of the nanotube. Moreover, carbon nanotubes can be either single-walled or multi-walled.

2.1 Electronic properties

The band structure of graphene is usually calculated using a tight-binding model and the resulting approximate dispersion relation is given by

$$E(\overrightarrow{k}) = \pm\gamma_1\sqrt{3 + 2\cos(\overrightarrow{k}\cdot\overrightarrow{a}_1) + 2\cos(\overrightarrow{k}\cdot\overrightarrow{a}_2) + \cos(\overrightarrow{k}\cdot(\overrightarrow{a}_2 - \overrightarrow{a}_1)}, \quad (2.1)$$

where the constant γ_1 comes from an overlap integral between the p_z atomic orbitals centered at the two atomic sites in each lattice cell respectively. The dispersion relation given by (2.1) is plotted in Figure 2.2. The K-points are sometimes called Dirac points since the dispersion relation around these exhibits a linear rather than quadratic behaviour with respect to the momentum. This fact alone is responsible for much of the peculiar electronic properties of the material. Graphene is considered to be a semi-metal since, in

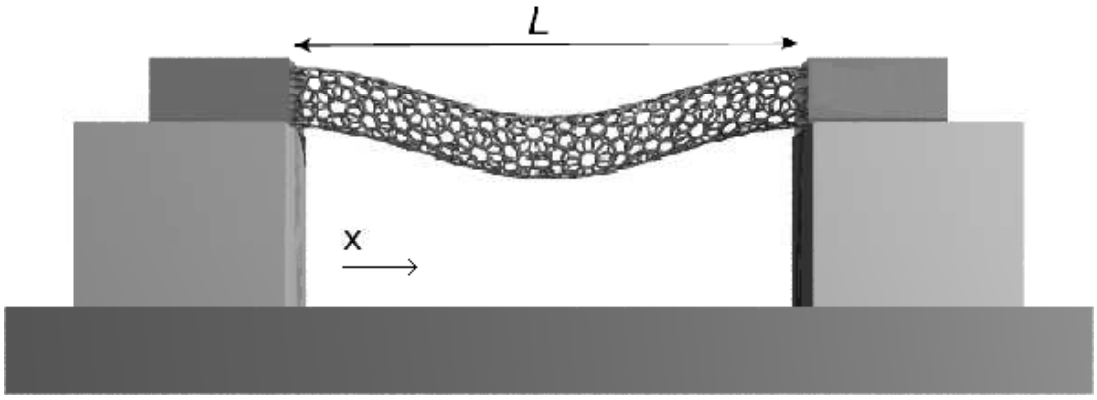

Figure 2.3: Illustration of a suspended Carbon Nanotube. Curtesy of Yury Tarakanov and Gustav Sonne.

spite of the absence of a bandgap, the density of states at the fermi level is zero. Hence, at zero temperature a perfect graphene sheet is in principal a non-conducting material. The conductivity can however be manipulated by either inserting impurities or through electronic doping by a gate electrode. The latter method, which is very important for our considerations, will be discussed more in later chapters. For a comprehensive review of the electronic properties of graphene see for example Ref [7].

The electronic band structures of different kinds of carbon nanotubes are obtained from that of graphene by imposing certain boundary conditions specified by the chirality of the tube. It turns out that there is a simple way of determining whether the carbon nanotube is metallic or semiconducting based on its chirality. If $m-n$ is an integer multiple of 3 then it is metallic, otherwise it is semiconducting. The explanation for this, together with a full treatment of the other transport properties, can be found in Ref [8].

2.2 Mechanical properties

The systems which we will consider consists in part of a mechanical resonator suspended in both of its ends over a trench. This setup, exemplified by a carbon nanotube, is depicted in figure (2.3). The equations governing the dynamics of the mechical resonator also differ depending on whether we consider a carbon nanotube or a graphene sheet. In particular the non-linear forces scale differently, something that will be important for the discussion in Chapter 7. If we first consider a carbon nanotube, the appropriate equation to use is the Euler-Bernoulli beam equation, which including a geometric non-linearity

term and an external force F_{ext} reads:

$$ES\frac{\partial^4 z}{\partial x^4} + \rho A\frac{\partial^2 z}{\partial t^2} + \gamma\frac{\partial z}{\partial t} = \left(\frac{EA}{2L}\int_0^L \left(\frac{\partial z}{\partial x}\right)^2 \mathrm{dx}\right)\frac{\partial^2 z}{\partial x^2} + F_{ext}. \tag{2.2}$$

Here E is the Young's modulus, ρ the mass density, A the cross sectional area, S the area moment of inertia, γ the damping coefficient and L the length of the nanotube. If we let r denote the radius of the nanotube we have that $A = \pi r^2$ and $S = \pi r^4/4$. For the kind of dynamical systems we will consider, the most rational way to deal with equation (2.2) is to express the vertical deflection as a series expansion

$$z(t,x) = \lambda\sum_n u_n(t)\phi_n(x/L). \tag{2.3}$$

Using the notation $\hat{x} = x/L$, the mode shapes are given by the expression

$$\begin{aligned}\phi_n(\hat{x}) =& C_n\{(\sin(k_n) - \sinh(k_n))(\cos(k_n\hat{x}) - \cosh(k_n\hat{x})) &(2.4)\\ &- (\cos(k_n) - \cosh(k_n))(\sin(k_n\hat{x}) - \sinh(k_n\hat{x})\}, &(2.5)\end{aligned}$$

where C_n are normalization constants chosen so that $\int_0^1 \phi_n(\hat{x})^2 d\hat{x} = 1$ and the constants k_n satisfy the equation $\cos(k_n)\cosh(k_n) = 1$. The corresponding vibrational frequencies are given by

$$\omega_n = k_n^2\sqrt{\frac{ES}{\rho A}}. \tag{2.6}$$

In many cases, it is sufficient to take into account only the fundamental mode ϕ_0. If we neglect the nonlinear force term, set the timescale to $\tau = \omega_0 t$ and project the fundamental mode onto equation (7.2) we obtain

$$\ddot{u}_0(\tau) + \tilde{\gamma}\dot{u}_0(\tau) + u_0(\tau) = \frac{L}{K\lambda}\int_0^1 \phi_0(\hat{x})F_{ext}\mathrm{d\hat{x}} \tag{2.7}$$

where $K = k_0^4 ES/L^3$ is the spring constant. The right hand side of course becomes particularly simple when the external force is almost uniform across the tube, which is the case for the Lorentz force that will play a central role in the following chapters. The constant $Q = 1/\tilde{\gamma}$ will be referred to as the quality factor of the nanotube. At the time of writing, nanotubes with a Q-factor as high as 10^6 have been reported, [9,10]. For further discussion on the mechanical properties and dynamics of carbon nanotubes see for example Ref [11,12].

At one occasion we will also briefly consider the mechanics of a suspended graphene sheet, see Figure (2.4). The complete derivation of the mechanics of graphene is to long to be covered here, but can be found for example in Ref [13]. After a few simplifications, for example that we only need to take

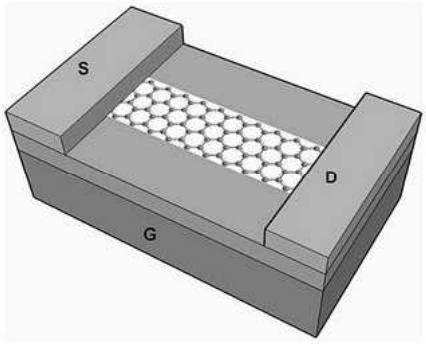

Figure 2.4: Illustration of a suspended Graphene Nanoribbon.

into account the vertical streching, the one-dimensional equation of motion of a doubly clamped graphene sheet reads

$$\rho\ddot{z}(t,x) + \rho\gamma\dot{z}(t,x) - T_0\partial_x^2 z(t,x) - T_1\partial_x\{(\partial_x z(t,x))^3\} = P_z(t,x), \tag{2.8}$$

where ρ is the area mass density of graphene, $P_z(t,x)$ is the pressure in the vertical direction, $T_0 = (\lambda + 2\mu)\delta$, $T_1 = \lambda/2 + \mu$, λ and μ being the so called Lamé-parameters and δ a parameter that quantifies the initial in-plane streching. For further discussion, see for example Ref [14].

CHAPTER 3

Sources of the Electro-Mechanical Coupling

There are two kinds of external forces F_{ext} that will occur throughout this thesis. The first is the electrostatic attraction between the charge on the nanotube and the charge on some external object placed in its vicinity, for example an STM-tip or a gate electrode. The second, and the one that will be given most attention, is the magnetically induced Lorentz force acting on moving charges inside the nanotube. The latter has the advantage that the direction of the force can be changed by simply adjusting the direction of the magnetic field. In order to couple the mechanical and electronic degrees of freedom we also need some mechanism in which the mechanical subsystem acts back on the electronic subsystem. The main feature that we will rely upon in every system geometry considered is some kind of sensitivity of the conductance of the carbon nanotube to its vertical displacement. There are a number of ways to obtain this sensitivity, some of which have already been analyzed theoretically and been observed in experiments. Before looking at these in more detail we first introduce what will later be referred to as the characteristic length scale of the system. For simplicity we assume that we only have to consider the fundamental bending mode with amplitude u. Moreover we assume that the resistance $R(u)$ of the nanowire is dependent on the amplitude, by some mechanism yet to be specified, and we define

$$\ell = -\frac{R(u)}{R'(u)}. \tag{3.1}$$

The characteristic length scale could be thought of as the distance the wire has to move from its stationary point of deflection in order for the resistance to be reduced to half of its original value. That is, the shorter ℓ the higher sensitivity. Important to remember is that this length scale is a 'local property' since in most cases it will depend on the stationary deflection. Hence, the characteristic length is not a property of the system geometry alone but may also depend on external parameters such as applied fields and other forcings.

3.0.1 Mechanical Strain

The natural starting point is perhaps to investigate the change in conductance of a carbon nanotube due to pure mechanical strain. The effect does indeed

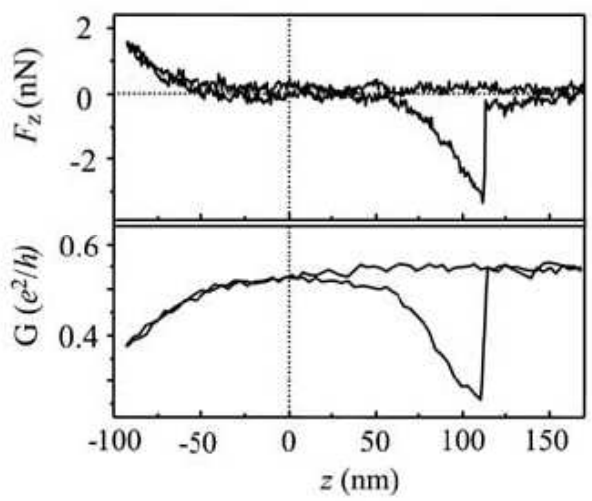

Figure 3.1: Graph taken from the paper [15] by E.D. Minot, Y. Yaish et. al., showing the conductance as a function of displacement for a 1.9 μm long metallic carbon nanotube with a diameter of 6.5 nm.

show up for a sufficiently large bending, something that was reported in the papers [15, 16] and later in [17]. In the experiments performed, the strain on the nanotube was applied through an atomic force microscope. The conductance of a particular metallic carbon nanotube as a function of mechanical bending is shown in Figure (3.1). As one can see, in this case the nanotube has to be bent approximately 50 nm (corresponding to approximately 3% ratio between the deflection and nanotube length) before the effect shows up clearly. From inspection of the graph we estimate the characteristic length scale for this coupling to be at best of the order of 100 nm but for practical purposes probably much longer. The reason why this reduction in conductance occurs is not completely settled. It has been suggested that the effect is due to a local distortion in the sp^2 bond, another suggestion is that there is an opening of a band gap. It should also be noted that for some nanotubes the conductance may increase due to mechanical strain. For further discussions on the topic we refer to the papers cited above.

3.0.2 Electronic Doping

The effect of electronic doping on the conductance of a semiconducting carbon nanotube has been investigated thoroughly in the papers [18,19] and [20]. The basic mechanism could be outlined as follows: An electrode (gate) is put in the vicinity of the nanotube and by adjusting the applied gate voltage one can controle the number of electronic carriers, which in turn affects the conductance of the nanotube, see Figure (3.2). In order to understand how the

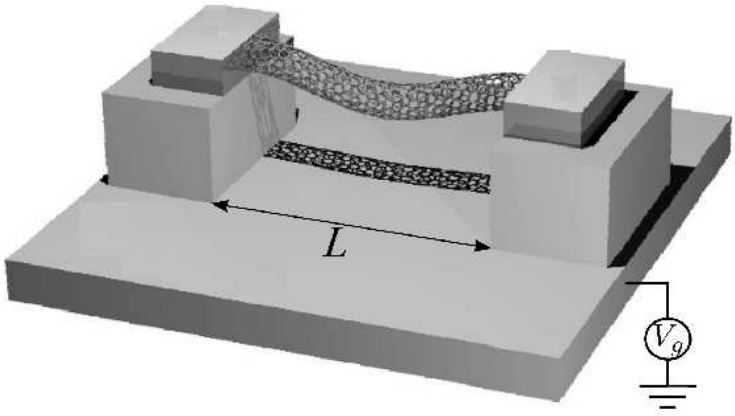

Figure 3.2: Illustration of a carbon nanotube suspended over a gate. Image used with the permission of Y. Tarakanov.

mechanical deflection of the nanowire comes into play we assume the charge on the tube to be simply the product of the gate voltage and the mutual capacitance between the nanotube and the gate: $q = V_g C_g$. Put in differential terms we have

$$\delta q = \delta V_g C_g + V_g \delta C_g. \tag{3.2}$$

The gate voltage is assumed to be fixed, which is why the first term on the right hand side disappears. However, the capacitance depends on the distance between the nanotube and the gate. This is why the charge and ultimately the conductance depends on the displacement of the nanotube. Experimental evidence of this phenomenon was reported in the paper of V. Sazonova, Y. Yaish et al. 'A tunable carbon nanotube electromechanical oscillator' [21]. In the cited paper the mechanism was utilized to detect the oscillating motion of the nanowire and thereby determine its resonance frequency. Experiments demonstrating the same effect have also been performed more recently, see for example [22, 23]. We expect the typical characteristic length scale for the electronic doping coupling to lie somewhere between 10^{-7} m and 10^{-6} m. For detailed calculations we refer to Appendix A. An almost identical analysis can be carried out for graphene, see Refs. [7, 24].

3.0.3 Electronic tunneling

The phenomenon of electronic tunneling would, if implemented sucessfully into our schemes, result in a very short characteristic length. If we imagine a system with an STM-tip positioned just a few tenths of a nanometer above the nanotube acting as the contact, see Figure 3.3, the conductance at the junction would be proportional to the propability of electrons tunneling between the STM-tip and the nanotube. This tunneling probability may change drasti-

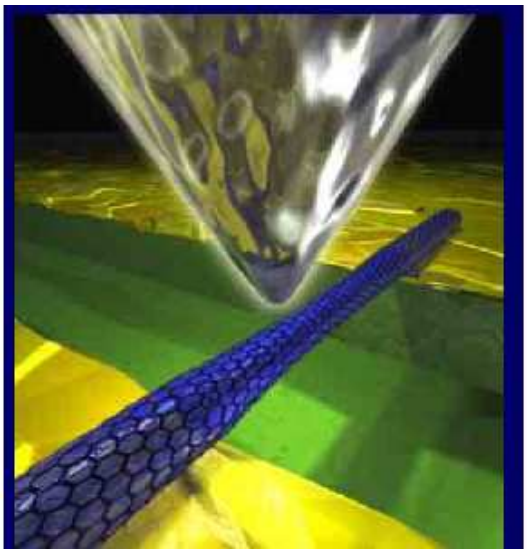

Figure 3.3: Illustration of an STM-tip positioned above a suspended carbon nanotube.

cally on a distance of just 0.1 nm. Despite its great sensitivity, implementing this kind of geometry poses some serious challenges since the amplitude of oscillation of the nanotube is greatly limited due to the short distance to the tip. There is a certain risk that if the nanotube hits the STM-tip it will remain attached to it because of some attractive force, for example a Van der Waals force. The system does however exhibit many interesting phenomena, and the coupling with mechanical degrees of freedom have attracted attention recently, see for example [25–27].

CHAPTER 4

Time Scales and I-V Characteristics

Before exploring the main material we will make a small departure to discuss some concepts that will be useful in the sequel. Let us for the moment think of our system as a black box with unknown composition. We may perform experiments on this box by sending some electronic input signal and then analyze the results in terms of voltage drop, current, current-voltage oscillations and so on. In this thesis we will consider two such inputs, or biases as they are commonly called. Those are voltage bias and current bias respectively. In the voltage bias regime the circuit is held at constant voltage drop and it is assumed that the resistance of the box is much larger than the resistance of the circuit connecting it to the voltage source. In the current bias regime, on the other hand, one end of the circuit is fed by a constant external current. Voltage bias is technically and conceptually more straighforward and it is what virtually all of our every day electric equipment operate under. Current bias is somewhat more complicated on the mesoscopic scale since ultimately you need a potential difference to accelerate the electrons. Technically it is accomplished by connecting the system to a voltage source in series with a resistance much larger than the resistance of the box. Due to the difference in resistance, almost the entire potential drop will reside over the external resistor so that the system 'feels' only an external current.

4.1 I-V Curves

So far we have not said anything about the interior of the box. It may be very simple, for example if it contains only a resistor. On the other hand it may also be complex with many coupled degrees of freedom. Our every day intuition tells us that if we increase the voltage bias the current through the circuit should increase. That would indeed be the case for an ordinary resistor. Correspondingly, in the current bias regime we expect the voltage drop over the box to increase if more charge is supplied. While this is true in most cases it need not be for a sufficiently complicated box. The way in which the current depends on voltage or vice versa is usually illustrated with so called I-V curves. In the voltage bias regime, if it happens that the current actually decreases with increasing voltage in some interval one speaks of an N-shaped I-V characteristic. Conversely, in the current bias regime, if the voltage drop

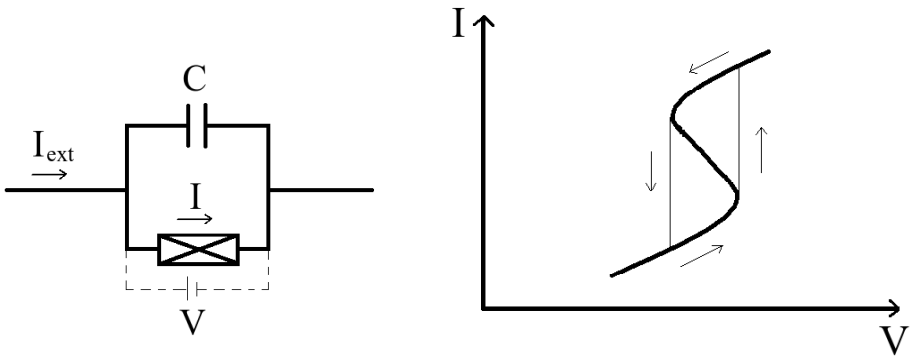

Figure 4.1: Schematic illustration of a system with an S-shaped I-V characteristic performing self-oscillations in the current bias regime.

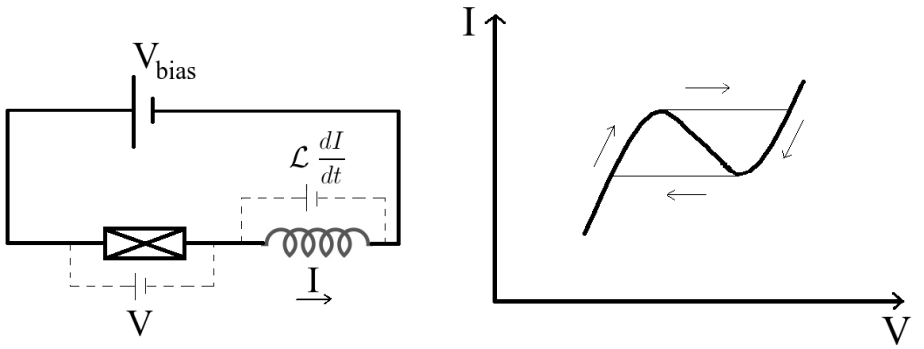

Figure 4.2: Schematic illustration of a system with an N-shaped I-V characteristic performing self-oscillations in the voltage bias regime.

decreases with increasing external current in some interval one speaks of an S-shaped I-V characteristic. Typically in the latter case the system can be made to perform current-voltage selfoscillations by connecting a sufficiently large capacitor in parallel to the box and applying an external current within the critical interval as illustrated in figure (4.1). To achieve selfoscillations in the case of an N-shaped I-V curve it is usually sufficient to connect a large enough inductor in series, see Figure (4.2). There are actually two sides of the coin for each of these I-V characteristics. Suppose you have a system which in the current bias regime yields an S-shaped I-V curve. If we then switch regime and apply a constant voltage in the interval of negative slope ($dV/dI < 0$) the system will exhibit a phenomenon called bi-stability. As can be seen from figure (4.3), in this case there are three different currents that correspond to the given voltage bias, two of which are stable in the sense that small deviations will not take the system far away from its stationary state. Many of the systems we will encounter have neither S-shaped nor N-shaped I-V curves. Indeed, these I-V

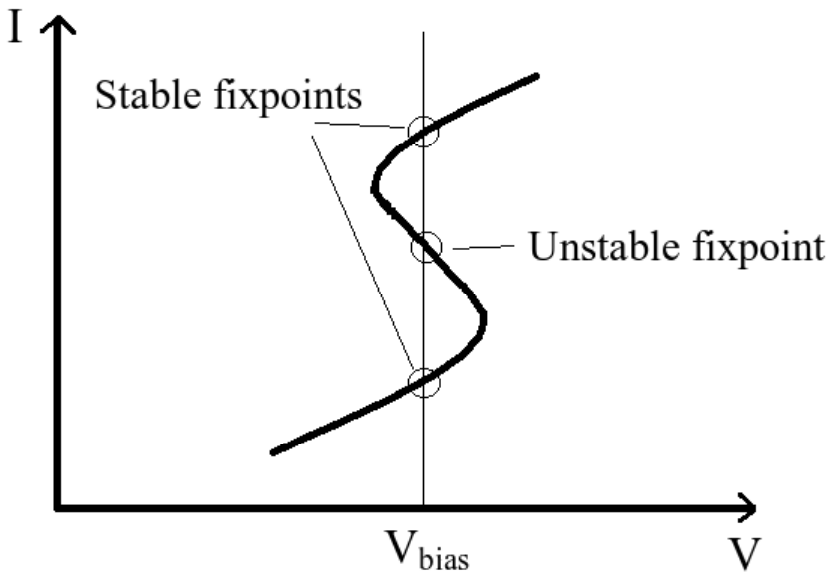

Figure 4.3: A system exhibiting an S-shaped I-V curve in the current bias regime which is now subject to a voltage bias within the critical interval. As illustrated, there are three different currents that correspond to the given voltage bias, two of which are stable in the sense that small deviations will not take the system far away from its stationary state.

characteristics are by no means necessary for the current and voltage to start to oscillate under constant forcing. The above discussion nevertheless serves a purpose in that it introduces some useful concepts and that it provides a tool to better understand the nature of the electro-mechanical instability. It might be the case that the instability is mainly caused by the mechanical (or some other) subsystem, and that the current voltage fluctuations are merely a reaction to the mechanical subsystem. If one concludes, however, that an S- or N-shaped I-V curve, (also sometimes called negative differential resistance), is necessary for self oscillations, that usually indicates that the instability mainly resides in the electronic subsystem.

4.2 Time Scales

In Chapter 2 we identified an important time scale, namely that corresponding to the mechanical frequency of oscillation ω_0. From elementary circuit theory we are also familiar with other characteristic time scales such as the relaxation time of an RC-circuit, with the corresponding frequency

$$\omega_R = 1/(RC). \tag{4.1}$$

Moreover, we have the frequency of an LC-circuit

$$\omega_L = 1/\sqrt{\mathcal{L}C}. \tag{4.2}$$

In the systems considered in the following chapter we will assume that there is a nonzero resistance and in most cases some effective capacitance, external and/or internal. The effective capacitance referred to here should not be confused with the gate capacitance mentioned in Section (3.0.2). In the case of voltage bias we will also assume that there is some effective inductance in the circuit, external and/or internal. We will see that the relationships between the mechanical and electronic time scales play a central role in the subsequent calculations.

CHAPTER 5
Magnetomotive Instability

Before we proceed we will make a brief summary of what we have discussed so far. We have identified three mechanisms or geometries in which the conductance of the CNT depends on the mechanical displacement: 1) Mechanical strain, 2) Electronic doping and 3) Electronic tunneling. To each mechanism is associated a certain characteristic length scale ℓ (which may depend on external parameters). Moreover we have discussed two different electronic feedbacks on the mechanical motion: 1) A magnetically induced Lorentz force which is proportional to the current through the nanotube and 2) An electrostatic attraction between the nanotube and some other object, typically an STM-tip. We have also discussed two different regimes under which these systems may operate: 1) Current bias regime and 2) Voltage bias regime. In pricipal one can combine these modes of operation in several different ways and from a practical point of view there are advantages and disadvanatges with each of these. The analysis has shown, however, that the most important is probably the voltage bias regime combined with Lorentz force feedback. The reason for this will hopefully become clear in the following three chapters. Here we will exclusively consider the Lorentz force feedback, starting with the mathematically simpler current bias regime.

5.1 Self oscillations in the current bias regime

Consider the setup depicted in figure (5.1). We have a suspended semiconducting CNT which is subject to an external current and a constant magnetic field. The direction of the magnetic field is of vital importance as we will explore later. How to model the mechanical motion has already been discussed in Chapter 2. Let us assume as before that we only need to consider the fundamenatal bending mode with a time dependent amplitude $u(t)$. The equation of motion then reads

$$m\ddot{u} + \gamma\dot{u} + ku = LHI_{cnt}. \tag{5.1}$$

The right hand side of equation (5.1) is the Lorentz force proportional to the current through the wire, where L denotes the effective length of the wire. In order to model the electronic part we first write the equation for the charge

$$\dot{q} = I_0 - I_{cnt}. \tag{5.2}$$

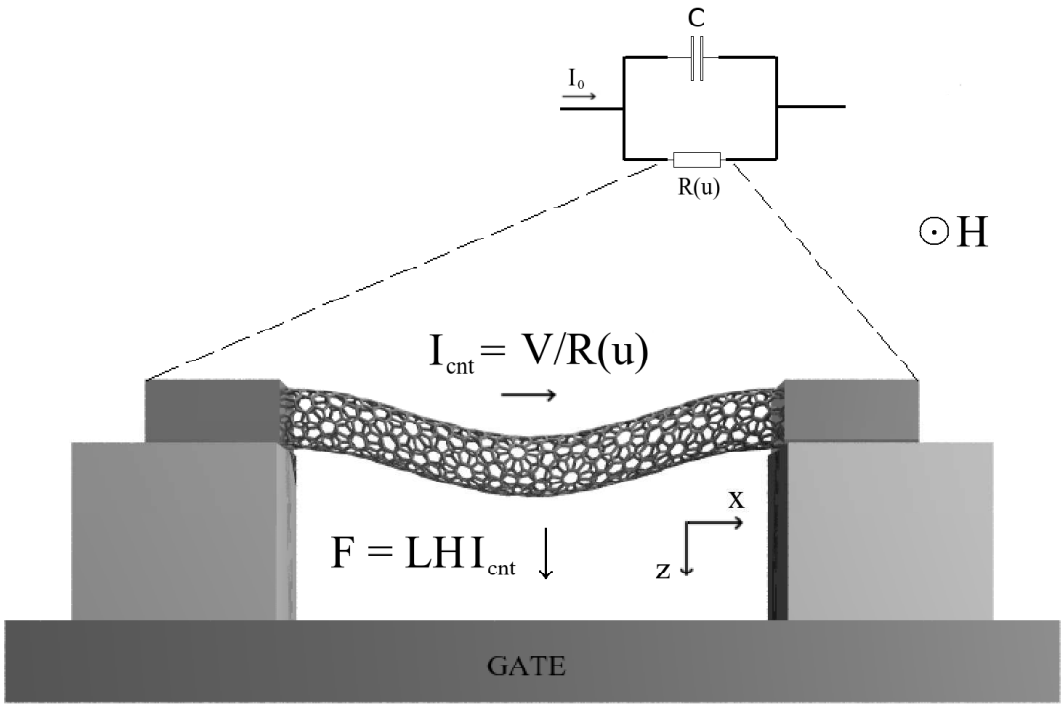

Figure 5.1: Sketch of the current biased oscillator device. A semiconducting carbon nanotube is suspended over a gate electrode and connected to an external dc current source. A uniform magnetic field, applied perpendicular to the direction of the current, gives rise to a Lorentz force that deflects the tube towards the gate. This affects the resistance and provides a feedback mechanism that for large enough magnetic fields leads to self-sustained nanotube oscillations. The inset shows an equivalent electric circuit of the device.

This simply states that the time derivative of the charge at the left lead is the charge provided per unit time by the external current minus the charge escaping through the wire per unit time. If we divide equation (5.2) by the capacitance we get the equivalent equation for the voltage

$$\dot{V} = \frac{1}{C}(I_0 - I_{cnt}). \tag{5.3}$$

What remains is an expression for the current through the wire, which is simply Ohm's law but now with a position dependent resistance:

$$I_{cnt} = \frac{V}{R(u)}. \tag{5.4}$$

For fixed external parameters there is a unique stationary solution ($\ddot{u} = 0$, $\dot{u} = 0$, $\dot{V} = 0$) to the above system of equations given by

$$V_0 = R(u_0)I_0, \tag{5.5}$$

$$u_0 = \frac{LHI_0}{k}. \tag{5.6}$$

In order to elucidate the role of all parameters involved it is convenient to switch to the dimensionless time

$$\tau = \omega_0 t, \tag{5.7}$$

and the dimensionless variables

$$\beta = u/\ell(u_0), \tag{5.8}$$

$$\varphi = V/V_0. \tag{5.9}$$

It is important to note that the scaling, except possibly the time scaling, depends on the stationary deflection. As length scale we have made use of the characteristic length introduced in Chapter 3 for which the dependence on u_0 is written explicitly. Furthermore, we introduce the dimensionless conductance:

$$f(\beta) = \frac{R_0}{R(\beta)}, \tag{5.10}$$

where R_0 simply denotes the resistance at the stationary point of deflection. The dimensioneless conductance has the desired property that $f(\beta_0) = f'(\beta_0) = 1$, ($\beta_0 = u_0/\ell(u_0)$). In dimensionless variables the system of equations can be expressed as

$$\ddot{\beta} + Q^{-1}\dot{\beta} + \beta = \beta_0\varphi f(\beta), \tag{5.11}$$

$$\dot{\varphi} = \frac{\omega_R}{\omega_0}(1 - \varphi f(\beta)).$$

The significance of the parameters introduced earlier have now become clearer. From a mathematical point of view there are only three parameters that define the system: (1) The electromechanical coupling parameter β_0, which also happens to be the stationary point of deflection in rescaled coordinates, (2) The quality factor Q and finally (3) The ratio between the electronic and mechanical frequences ω_R/ω_0 (where $\omega_R = 1/(R_0C)$). Expressed in physical parameters, the electromechanical coupling parameter for this particular system is given by

$$\beta_0 = \frac{LHI_0}{k\ell(u_0)}. \tag{5.12}$$

In order to find the necessary conditions for instability the most straightforward procedure in this case is to perform a linear stability analysis, a method which is outlined in Appendix B. It is sometimes possible to obtain exact expressions if the dimension of the system is sufficiently low. Indeed, for the system (5.11) we have the following exact criterion for instability:

$$\beta_0 > \beta_c = \frac{1}{Q}\frac{\omega_0\omega_R + Q(\omega_0^2 + \omega_R^2)}{\omega_0(\omega_0 + Q\omega_R)}. \tag{5.13}$$

In the limit of high quality factors we have the somewhat simpler expression

$$\beta_0 > \beta_c \approxeq \frac{1}{Q}\left(\frac{\omega_R}{\omega_0} + \frac{\omega_0}{\omega_R}\right). \tag{5.14}$$

Clearly, the system's succeptability to selfexcitations increases as the characteristic frequencies ω_0 and ω_R approach each other. This kind of limiting value where the quality factor competes against the ratio between two characteristic timescales will occur frequently throughout the remainder of this thesis. We may now return to the question touched upon before, namely in which direction to orient the magnetic field. The answer lies implicit in the formulas just derived but may not be self evident. If we recall the definition of the characteristic length scale, there is a sign convention that defines the positive β-direction as the direction towards increasing conductance, or equivalently, decreasing resistance. Since the critical value β_c is always positive for this setup it means that in order to obtain instability the magnetic field has to be directed so as to push the carbon nanotube towards increasing conductance. The latter is not always the case as we will see in the next section. The formulas which we have derived so far does not provide any information on how the instability evolves in time. The first question to adress is the shape of the I-V curve discussed in Chapter 4. For this purpose it is useful to return to the equations for the stationary solution in original variables:

$$V_0 = R(u_0)I_0, \tag{5.15}$$

$$u_0 = \frac{LHI_0}{k}. \tag{5.16}$$

For nonzero magnetic field, u_0 can be used as a parametrization of V_0 and I_0 and we may write the derivative dV_0/dI_0 as

$$\frac{dV_0}{dI_0} = \frac{dV_0}{du_0}\frac{du_0}{dI_0} = \left(I_0 R'(u_0) + R(u_0)\frac{dI_0}{du_0}\right)\frac{du_0}{dI_0}. \tag{5.17}$$

From this follows that

$$\frac{dV_0}{dI_0} < 0 \iff \beta_0 = \beta_0(I_0) > 1. \tag{5.18}$$

This means that the slope is negative precisely when $\beta_0 > 1$ yielding an S-shaped I-V curve. Upon inspection we also see that in this situation there is indeed one and only one critical capacitance, since $\beta_c \to 1$ as $\omega_R \to 0$ (which corresponds to the limit $C \to \infty$). Moreover, from the discussion in Chapter 4 we also know that from an S-shaped I-V curve we can have bistability if we change to voltage bias, but that is another story. A situation with such a high coupling parameter must however be considered rare and in a more realistic situation we would expect $\beta_0 \ll 1$. In this case the time-evolution can be studied analytically by making the ansatz $\beta = \beta_0 + A(\tau)\sin(\omega\tau)$, assuming $A(\tau)$ to be a slowly varying function on the timescale of the rapid oscillations, and solve for φ by a perturbation expansion $\varphi = 1 + A\varphi_1 + A^2\varphi_2 + A^3\varphi_3 + \cdots$, see [28]. Despite the fact that the system has only three dimensions the calculations beyond second order are somewhat cumbersome. There is however the phenomenon of a deviation of the average voltage from its stationary value which can be understood as the occurence of constant terms in the perturbation expansion of φ. The lowest order constant term is found to be proportional to A^2 and if we let A_s denote the saturation amplitude of the mechanical oscillation then for small A_s the voltage drop (rise) can be approximated by

$$\frac{V_{av} - V_0}{V_0} \approx \frac{2 - (1 + \omega_0^2/\omega_R^2)f''(\beta_0)}{4(1 + \omega_0^2/\omega_R^2)}A_s^2. \tag{5.19}$$

This phenomenon can be seen clearly from the computer simulation presented in figure (5.2).

Using the same technique we can derive an equation for the time evolution of the amplitude:

$$\dot{A}(t) = a_1\omega_0 A(t)\left[\left(\frac{\beta - \beta_c}{\beta}\right) + b_1\frac{A^2(t)}{(2\ell_R)^2}\right], \tag{5.20}$$

where

$$\begin{aligned} a_1 &= \frac{\beta}{2}\frac{\omega_0\omega_R}{\omega_0^2 + \omega_R^2} \\ b_1 &= \frac{4\omega_0^4 - 5\omega_0^2\omega_R^2 + 3\omega_R^4}{2(\omega_0^2 + \omega_R^2)(4\omega_0^2 + \omega_R^2)} + \\ &\quad + \frac{1}{2}\left(\frac{3\omega_R^2 - \omega_0^2}{\omega_0^2 + \omega_R^2}\right)\frac{\partial \ell_R}{\partial u_0} - \frac{1}{2}\ell_R\frac{\partial^2 \ell_R}{\partial u_0^2}. \end{aligned} \tag{5.21}$$

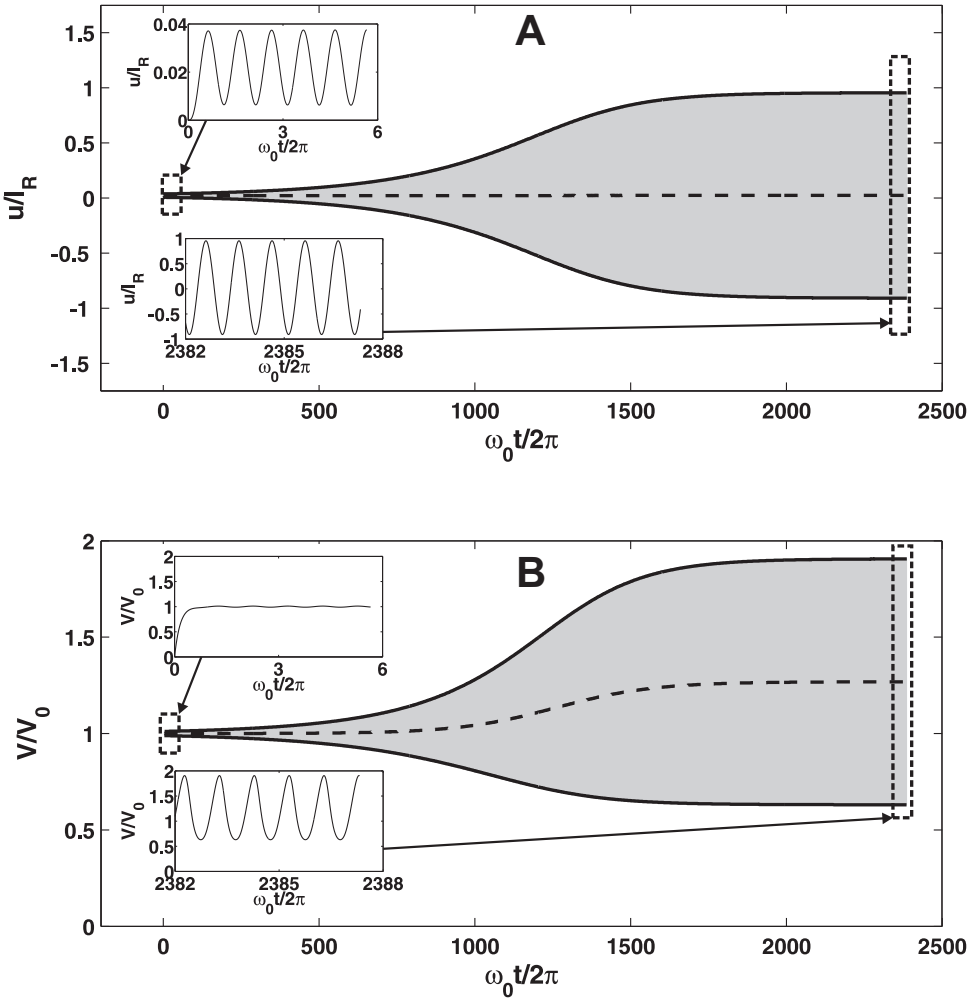

Figure 5.2: Time evolution of (A) the mechanical deflection of a suspended carbon nanotube and (B) the voltage drop over a vibrating nanotube of quality factor $Q = 100$ and resistance $R(u)/R_0 = (1 + e^{-2(u-u_0)/\ell_R})/2$, as calculated from Eqs. (5.1) and (5.3) for the RC-frequency $\omega_R = \omega_0$, the coupling parameter $\beta_0 = 1.1\beta_c = 0.0219$, and the initial conditions $u(0) = 0$, $\dot{u}(0) = 0$, and $V(0) = 0$. The grey areas span the envelopes of the unresolved oscillations while the dashed lines mark their time averaged values. As can be seen, the time averaged voltage drop deviates more and more from the static value V_0 as the amplitude of the mechanical oscillation increases. Image created by Yury Tarakanov, [29].

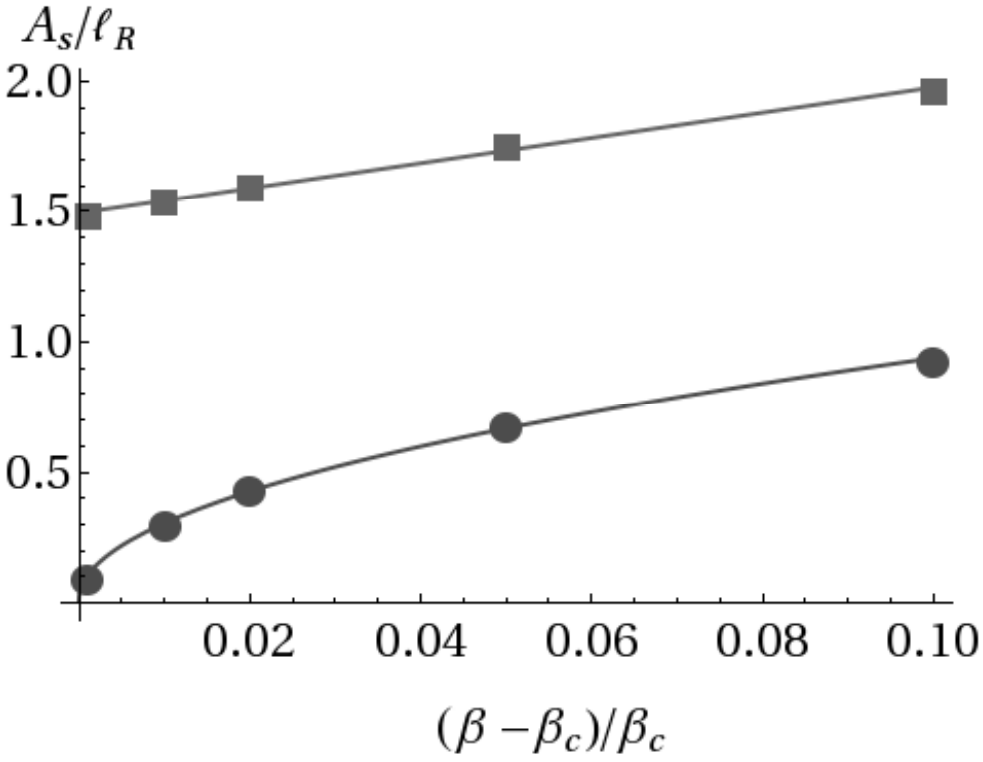

Figure 5.3: Saturation amplitude A_s, normalized to the characteristic length ℓ_R, for a carbon nanotube of quality factor $Q = 100$ and resistance $R(u)/R_0 = (1 + e^{-2(u-u_0)/\ell_R})/2$, as calculated from Eqs. (5.1) and (5.2) using the initial conditions $u(0) = 0$, $\dot{u}(0) = 0$, and $V(0) = 0$. Results in the "soft" instability regime ($\omega_R = \omega_0$) for different values of the coupling parameter β, which are all larger than than but close to the critical onset value β_c, are marked by solid circles while solid squares are used to mark results in the "hard" instability regime ($\omega_R = 2\omega_0$). The solid lines are guides for the eye.

The main significance of Formula (5.21) is that if the coefficient b_1 is negative, then we can predict the saturation amplitude as the solution of a second order algebraic equation. In the opposite case, however, there is no stationary solution and one would have to continue the perturbation expansion to higher orders, which in practise is almost an impossibility. These two cases, which are illustrated in Figure (5.3) corresponds to two different types of instability which we call soft- and hard instability respectively. In the case of soft instability, which in our case is most likely to occur for relatively low ω_R, it is in principle possible to, through the strength of the magnetic field, adjust the saturation amplitude to a value arbitrarily close to zero.

5.2 Self oscillations in the voltage bias regime

We will now consider a similar oscillator device which instead of an external current source is driven by a constant voltage bias V_0. In order to achieve self-oscillations in this regime it is necessary that there be some inductance $\mathcal{L}$ in the circuit, which we assume can be represented by an external inductor in series with the CNT, see figure (5.4).

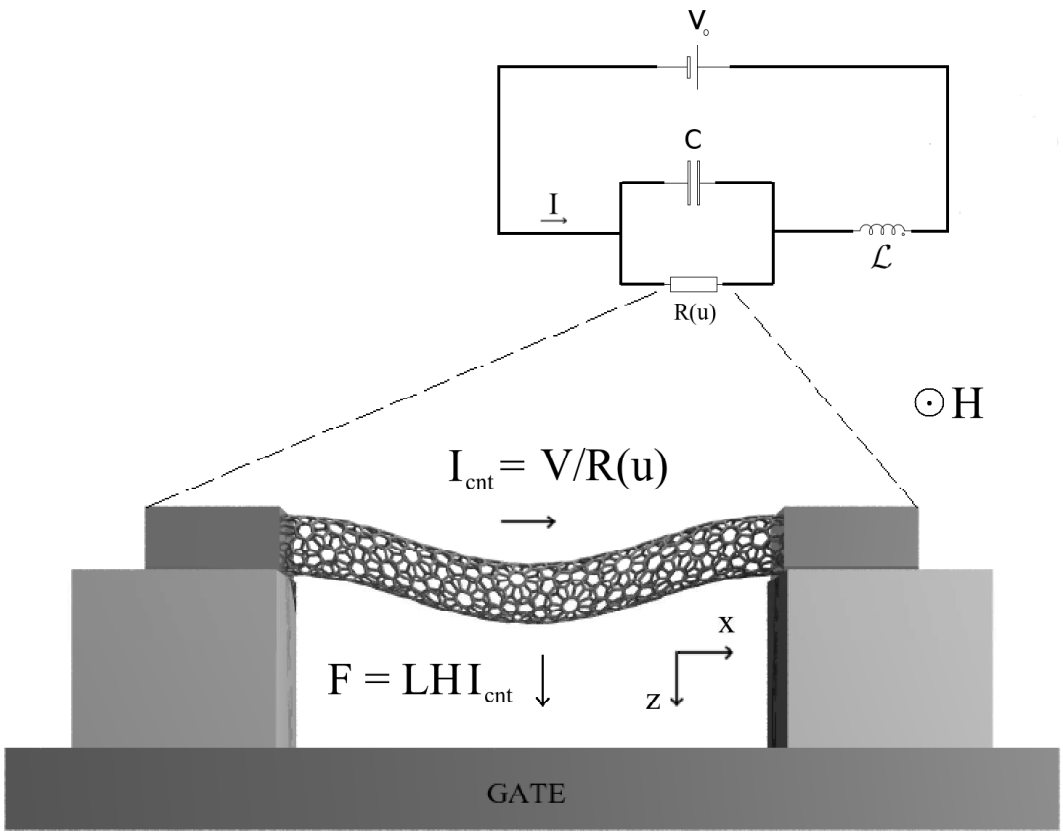

Figure 5.4: Sketch of the voltage biased oscillator device. A semiconducting or metallic carbon nanotube is suspended over a gate electrode and connected to an external dc voltage source. A uniform magnetic field, applied perpendicular to the direction of the current, gives rise to a Lorentz force that deflects the tube away from or towards the gate electrode. Which direction that can give rise to selfexcitations is determined by the ratio ω_L/ω_0 (see text). The inset shows an equivalent electric circuit of the device.

It is now important to distinguish between the voltage bias V_0 on the one hand and the voltage drop over the CNT which as before will be denoted V. The current through the CNT is denoted I_{cnt} while the current through the inductor, which is the sum of I_{cnt} and the capacitive current, is denoted I. The

dynamics of this system is governed by the equations:

$$\begin{aligned} &m\ddot{u} + \gamma\dot{u} + ku = LHV/R(u), \\ &\dot{V} = \frac{1}{C}(I - I_{cnt}), \\ &V_0 - V - \mathcal{L}\dot{I} = 0. \end{aligned} \tag{5.22}$$

The last equation, which simply states that the total voltage drop over the circuit be zero, determines the time evolution of the current. A stationary solution to (5.22) must satisfy the equations

$$I_0 = V_0/R(u_0), \tag{5.23}$$

$$u_0 = \frac{LHI_0}{k}, \tag{5.24}$$

and as we can see, in the voltage bias regime it need not be unique. Switching to the dimensionless parameters

$$\begin{aligned} &\tau = \omega_0 t, \\ &\beta = u/\ell(u_0), \\ &\varphi = V/V_0, \\ &\psi = I/I_0, \end{aligned} \tag{5.25}$$

the system of equations may be written

$$\begin{aligned} &\ddot{\beta} + Q^{-1}\dot{\beta} + \beta = \beta_0\varphi f(\beta), \\ &\dot{\varphi} = \frac{\omega_R}{\omega_0}(\psi - \varphi f(\beta)), \\ &\dot{\psi} = \frac{\omega_L^2}{\omega_R\omega_0}(1 - \varphi), \end{aligned} \tag{5.26}$$

where $f(\beta)$ is the dimensionless conductance defined by equation (5.10), $\omega_L = 1/\sqrt{\mathcal{L}C}$ is the LC-frequency and

$$\beta_0 = \frac{LHV_0/R_0}{k\ell(u_0)}. \tag{5.27}$$

This four-dimensional system can be analyzed by the same techniques used before, though resulting in somewhat more complicated expressions. The condition for *stability* is given by the two inequalities

$$\delta - F(\beta_0) < \beta_0 < \delta + F(\beta_0), \tag{5.28}$$

where

$$\delta = 1 + \frac{1}{Q}\frac{\omega_R}{\omega_0} + \frac{\omega_L^2}{\omega_0^2} - 2\frac{\omega_R/\omega_0 + \omega_L^2/(\omega_0^2 Q)}{\omega_R/\omega_0 + 1/Q}, \tag{5.29}$$

$$F(\beta_0) = \sqrt{(1 + \omega_R/(\omega_0 Q) + \omega_L^2/\omega_0^2 - \beta_0)^2 - 4(\omega_L^2/\omega_0^2)(1 - \beta_0)}. \tag{5.30}$$

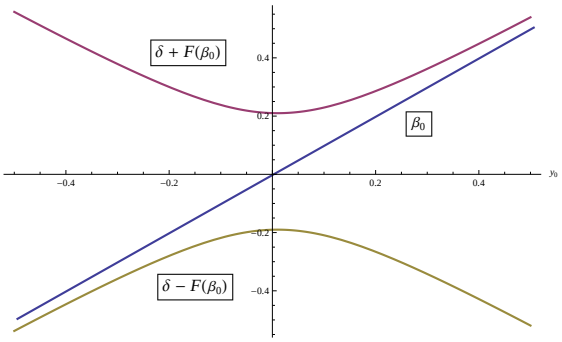

(a) $Q = 100, \omega_0 = \omega_R = \omega_L$. No region of instability.

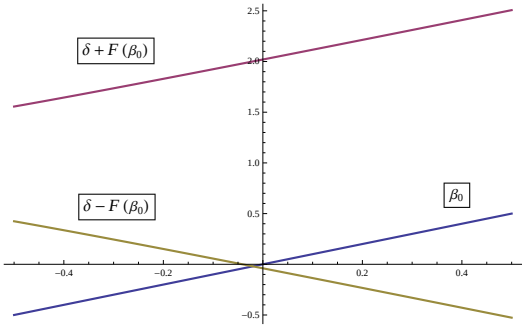

(b) $Q = 100, \omega_0 = \omega_R, \omega_L^2 = 2\omega_0^2$. $\beta_c < 0$.

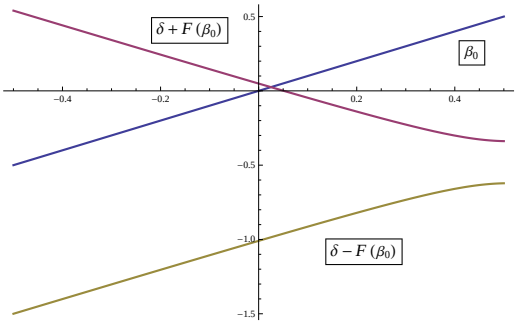

(c) $Q = 100, \omega_0 = \omega_R, \omega_L^2 = 0.5\omega_0^2$. $\beta_c > 0$.

Figure 5.5: Graphs of the functions $\delta + F(\beta_0)$, β_0 and $\delta - F(\beta_0)$ for different system parameters. Instability obtains when either of the two inequalities $\delta - F(\beta_0) < \beta_0 < \delta + F(\beta_0)$ is reversed. See the text for details.

Hence, selfexcitations will occur when either of these inequalities is reversed. However, for fixed system parameters ($\omega_0, \omega_R, \omega_L, Q$) only one (if any) of these inequalities can be reversed by varying β_0 through the magnetic field. One can show that the instability condition boils down to

$$|\beta_0| > |\beta_c|, \quad \mathrm{Sgn}(\beta_0) = \mathrm{Sgn}(\beta_c), \tag{5.31}$$

where the critical electro-mechanical coupling parameter β_c is given by

$$\beta_c = -\frac{1}{Q}\left(\frac{\omega_L^2 - \omega_0^2}{\omega_R\omega_0 + \omega_0^2/Q} + \frac{\omega_L^2/Q + \omega_R\omega_0}{\omega_L^2 - \omega_0^2}\right). \tag{5.32}$$

We may now identify three cases: (1) If $\omega_0 = \omega_L$ there cannot be any instability regardless of the value of β_0. This singular behaviour is illustrated in Figure $(5.5(a))$. (2) If $\omega_L > \omega_0$ we have instability for $\beta_0 < \beta_c$ with β_c negative, see Figure $(5.5(b))$. (3) If $\omega_L < \omega_0$ we have instability for $\beta_0 > \beta_c$ with β_c positive, see Figure $(5.5(c))$. As mentioned before, the physical interpretation of the sign of β_0 is that if it is negative the carbon nanotube is pushed towards increasing resistance and if it is positive the nanotube is pushed towards decreasing resistance. This circumstance might be of importance if we wish to

utilize the effect of pure mechanical strain on the resistance. In this case the deflection dependence of the resistance is symmetric around the straight equilibrium configuration of the nanotube, hence, the sign of β cannot be reversed by simply changing the direction of the magnetic field. Moreover, for metallic nanotubes the resistance is indeed likely to increase with bending as already noted in Chapter 3, see [15], [17]. If we let the capacitance go to zero equation (5.32) reduces to

$$\beta_c = -\frac{1}{Q}\left(\frac{R_0}{\mathcal{L}\omega_0} + \frac{\mathcal{L}\omega_0}{R_0} + \frac{1}{Q}\right), \tag{5.33}$$

which is the same value one would obtain for the three-dimensional dynamical system

$$\begin{aligned} &\ddot{\beta} + Q^{-1}\dot{\beta} + \beta = \beta_0\psi, \\ &\dot{\psi} = \frac{R_0}{\mathcal{L}\omega_0}(1 - \psi/f(\beta)). \end{aligned} \tag{5.34}$$

Thus, by letting the capacitance go to zero we have in effect excluded the charge as a variable of the system and the relation between the voltage drop over the nanotube and the current is simply given by Ohm Law: $V = IR(u)$. By direct comparison with equations (5.11) and (5.19), for the system (5.34) we get the corresponding estimate for the deviation of the time averaged current I_{av} from the static value I_0 as a function of mechanical saturation amplitude A_s:

$$\frac{I_{av} - I_0}{I_0} \approx \frac{2 - (1 + (\mathcal{L}\omega_0)^2/R_0^2)(2 - f''(\beta_0))}{4(1 + (\mathcal{L}\omega_0)^2/R_0^2)} A_s^2. \tag{5.35}$$

An increase in the effective resistance, which in the voltage bias regime manifests itself as a reduction in time averaged current, appears to be a common feature of many self-oscillation occurences reported in the litterature. In Ref [30], by S. Perisau et al., the authors describe the deviation in timeaveraged current observed in experiments perfomed on singly clamped carbon nanotubes in a field emission environment:

'..It is always in the same direction: the current decreases when the nanowire enters into self oscillation and increases when it stops self oscillating. This counter intuitive and intriguing phenomenon also appears in a wide range of fields such as physiology, biology, hydrodynamics and electronics..'

If, in our case, we assume that $f''(\beta_0) = 0$ then we will indeed only observe a decrease in the averaged current. As we will see in Chapter 9 though, from theoretical considerations there may very well be situations when the time averaged current in fact increases due to mechanical self-oscillation.

CHAPTER 6

Cooling

One of the major advantages with the Lorentz force feedback is that the electromechanical coupling parameter can be controlled in magnitude by an external field that does not interfere too much with the other system parameters. Apart from this, in most cases one can switch the sign of the coupling parameter by simply reversing the direction of the magnetic field. As elucidated in the previous sections, selfexcitations can only occur if the coupling parameter has a certain sign, and a natural question arises what would be the effect on the mechanical motion if the sign was switched. The answer is, not surprisingly, that the spontaneous motion of the nanowire would be damped. This may open up the possibility to use the same setup as a device for 'cooling' the nanowire, in the sense that its spontaneous motion is reduced below the magnitude that would obtain as a result of thermodynamic equilibrium with the environment. The idea to cool a nanowire by coupling its mechanical motion to an electronic subsystem via a magnetic field is not new and has been explored for example in the papers [31–34]. The ultimate goal of cooling is to reduce the motion of the nanowire to its quantum mechanical ground state. Such a pursuit needs a quantum mechanical treatment and the systems at hand cannot easily be formulated in that framework, mainly because we have included a resistance.

The question whether 'damping' automatically results in 'cooling' and in that case how much could be disputed. The answer very much depends on the implicit assumptions of the model, something which we will try to clarify in the following. A classical treatment of a harmonic oscillator coupled to a thermal bath consists usually of a stochastic differential equation, whose general form mathematicians often express in the following way:

$$dX = b(X,t)dt + B(X,t)dW \tag{6.1}$$

$$X(0) = X_0 \tag{6.2}$$

where X is the vector whose trajectory we wish to obtain and $W(t)$ stands for the so called 'Wiener process' or 'Brownian motion', which is defined by the following properties

$$W(0) = 0, \tag{6.3}$$

$$W(t+\Delta t) - W(t) \in N(0,\Delta t), \tag{6.4}$$

and that for all times $t_1 < t_2 < ... < t_{n-1} < t_n$ the random increments $W(t_2) - W(t_1), ..., W(t_n) - W(t_{n-1})$ are independent. The formulas (6.1) immediately suggest an Euler type numerical implementation, where for a given time step dt we simply replace dW by $N(0,1)\sqrt{dt}$. Later on we will compare our analytical estimates with computations of this kind. Considering now a harmonic oscillator coupled to a thermal bath, the standard classical model is

$$m\ddot{u} + \gamma\dot{u} + ku = \sigma\xi(t), \tag{6.5}$$

where $\xi(t)$ is a stochastic force which in some sense represents the 'derivative' of the Wiener process. In particular we have that

$$\langle \xi(t) \rangle_\xi = 0 \tag{6.6}$$
$$\langle \xi(t)\xi(t') \rangle_\xi = \delta(t - t'). \tag{6.7}$$

Given these assumptions it is now a pure mathematical fact that

$$m\langle \dot{u}^2 \rangle = k\langle u^2 \rangle = \frac{\sigma^2}{2\gamma}. \tag{6.8}$$

It is thus evident that the stationary state is in some sense the result of a dualism between the diffusion term which will drive the oscillator if it has become too 'cold', and the dissipation term which will bring it down if it has become too 'warm' or excited. The conceptual twist comes when we try to reconsile this with the canonical equipartition theorem $k\langle u^2 \rangle = k_B T$, which forces us to put

$$\sigma^2 = 2k_B T\gamma, \tag{6.9}$$

which introduces a somewhat ad-hoc dependence between the two parameter σ and γ. In the following we will though treat σ and γ as independent. When estimating the cooling or heating caused by coupling the nanotube to an electronic subsystem we will do so by analyzing its effect in terms of a perturbation of the relevant parameters. Since the electronic subsystem is assumed to belong to the 'deterministic' part of the dynamics, the parameter in question is γ. If we define the effective temperature as $T_{eff} = k\langle u^2 \rangle / k_B$ and assume that the electronic coupling causes a shift in the dissipation term $\gamma \to \gamma'$, then, (assuming σ remains constant), the cooling coefficient is simply given by

$$\frac{T_{eff}}{T_0} = \frac{\gamma}{\gamma'}, \tag{6.10}$$

where T_0 is the environmental temperature. The question is now which γ we are actually competing against. If the nanotube is excited above thermal equilibrium the natural choise would be $\gamma = Q^{-1}$ so we will assume that this holds also below thermal equilibrium, though, given the previous discussion, it is by no means self evident. Considering again the system of equations for

the voltage biased device described in the previous chapter, but now with a stochastic force added to it:

$$\ddot{\beta} + Q^{-1}\dot{\beta} + \beta = \beta_0\varphi f(\beta) + \sigma\xi(t), \tag{6.11}$$

$$\dot{\varphi} = \frac{\omega_R}{\omega_0}(\psi - \varphi f(\beta)), \tag{6.12}$$

$$\dot{\psi} = \frac{\omega_L^2}{\omega_R\omega_0}(1 - \varphi), \tag{6.13}$$

there are at least two different ways to approach the problem. The one we will cover first is the more simpler and suggestive but with a more limited scope, which is shown in Appendix C. As mentioned in the previous chapter, if $|\beta_0| \ll 1$ we can assume that the mechanical motion follows a sinusoidal path $\beta(\tau) = A(\tau)\sin(\tau)$ where the amplitude $A(\tau)$ varies slowly on the time scale of the rapid oscillations. We then make the Ansätze $\varphi = \varphi_0 + A\varphi_1 + A^2\varphi_2 + ...$, $\psi = \psi_0 + A\psi_1 + A^2\psi_2 + ...$ and put them into the equations (6.12 - 6.13) and solve for each power of A successively [28, 35]. Given these solutions, if we equate the cosine terms to the first power of A on both sides of equation (6.11) we get the following expression for $\dot{A}$:

$$2\dot{A} = -(\beta_0 S + Q^{-1})A, \tag{6.14}$$

$$S = \frac{\omega_0\omega_R(\omega_L^2/\omega_0^2 - 1)}{\omega_0^2(\omega_L^2/\omega_0^2 - 1)^2 + \omega_R^2}. \tag{6.15}$$

Thus, the cooling coefficient becomes

$$\left(\frac{T_{eff}}{T_0}\right)_{VB} = \left(1 + \beta_0 Q\frac{\omega_0\omega_R(\omega_L^2/\omega_0^2 - 1)}{\omega_0^2(\omega_L^2/\omega_0^2 - 1) + \omega_R^2}\right)^{-1}. \tag{6.16}$$

The same conclution can be drawn by doing a perturbation analysis on the roots of the characteristic equation, something that is dicussed further in Appendix C. In principal the formula holds also if $\beta_0 S < 0$ but the result is then heating instead of cooling. The efficiency of either effect is dependent on the magnitude of the succeptibility S, which attains its absolute maximum of $1/2$ when

$$\omega_0\omega_R = |\omega_L^2 - \omega_0^2|. \tag{6.17}$$

One important thing to notice is that the sign of S depends on the relative magnitude of ω_0 and ω_L, something that will form the basis for the analysis carried out in Chapter 7 on selective self-excitation. It should also be noted that the succeptibility is zero precisely when $\omega_0 = \omega_L$. A computer simulation aimed at illustrating the cooling process is shown in Figure (6.1). A completely analogous treatment of the current biased device results in the cooling coefficient

$$\left(\frac{T_{eff}}{T_0}\right)_{CB} = \left(1 - \beta_0 Q\frac{\omega_0\omega_R}{\omega_0^2 + \omega_R^2}\right)^{-1}, \tag{6.18}$$

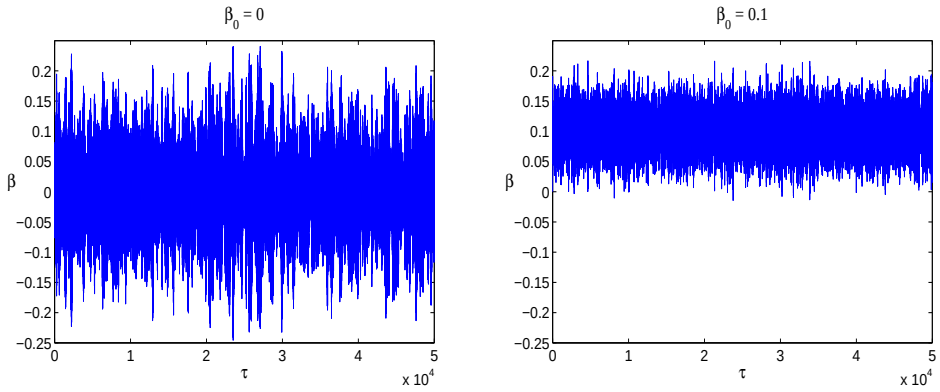

Figure 6.1: The figures display the results of two computer simulations of the system of equations (6.11 - 6.13) with the stochastic force $\sigma\xi(t) \in N(0, 0.01)$. The parameter values were $\omega_L = 2\omega_0$, $\omega_R = 3\omega_0$, $Q = 100$ and $f(\beta) = (1 - \exp(-2(\beta - \beta_0))/2$. The figure to the left shows a simulation with $\beta_0 = 0$ and the figure to the right shows a simulation with $\beta_0 = 0.1$. A numerical cooling coefficient of $(T_{eff}/T_0)_n \approx 0.19$ was obtained which is to be compared with the analytical result $(T_{eff}/T_0)_a = 1/6 \approx 0.17$.

Just as in the case of selfexcitations, we see that the efficiency is highest when $\omega_0 = \omega_R$, but important to notice is that the relative magnitude of ω_0 and ω_R does not affect the sign of the succeptibility function.

CHAPTER 7

Selective self-excitation of higher vibrational modes

In the previous chapters only the fundamental bending mode of the mechanical resonator was taken into account. However, by considering also the higher harmonics a carbon nanotube or a graphene sheet could be viewed as an infinite set of mechanical oscillators with frequencies $\omega_0, \omega_1, \omega_2, ...$ and so on. In order to include these modes we will step by step generalize some of the concepts introduced earlier, beginning with the mode dependent succeptibility function for the voltage biased device, which reads:

$$S_n = \frac{\omega_n \omega_R (\omega_L^2/\omega_n^2 - 1)}{\omega_n^2 (\omega_L^2/\omega_n^2 - 1)^2 + \omega_R^2}. \tag{7.1}$$

It is obvious that S_n will be negative for all n such that $\omega_n > \omega_L$ and positive for all n such that $\omega_n < \omega_L$. This simple observation forms the basis for this entire chapter. If we treat ω_L as a freely adjustable parameter then theoretically this opens up the possibility to excite an arbitrarily high overtone of a carbon nanotube, while at the same time the lower harmonics are kept relatively silent. This will be referred to as selective self-excitation. For previous theoretical work on this topic see for example [26, 27]. Experimentally, selective self-excitation has been achieved through photothermal actuation, as reported in the papers [36, 37]. In our case, it is worth to emphasize that

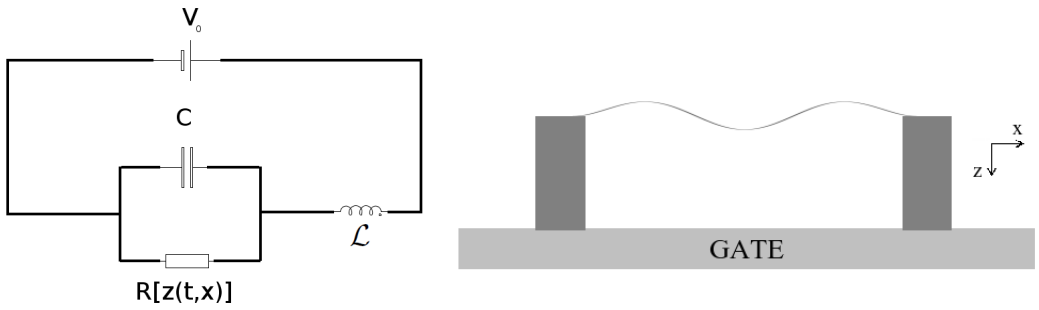

(a) (b)

Figure 7.1: Sketch of the proposed electronic circuit ($7.1(a)$). The resistor is comprised of either a graphene sheet or a carbon nanotube suspended over a gate electrode ($7.1(b)$).

for this to be possible we really need to be in the voltage bias regime. As

we will explore, there are several contributing factors that make the higher harmonics substantially less prone to become unstable, hence, without this frequency cut-off it is most likely that the fundamental bending mode would be excited and possibly even drive the system into a chaotic regime long before the higher mode in question has even reached the threshold of instability. The major complications that arise here is due to various intermode crosstalk which could be mediated either through fluctuations in the resistance but also through non-linear mechanical forces. In this chapter our model will therefore be extended to include these forces and we base our conclusions mainly on numerical simulations. We will also further discuss the material properties of carbon nanotubes and compare them with those of graphene.

7.1 Carbon nanotubes

We recall the dynamic equations for a doubly clamped elastic beam affected by a Lorentz force:

$$ES\frac{\partial^4 z}{\partial x^4} + \rho A\frac{\partial^2 z}{\partial t^2} + \gamma\frac{\partial z}{\partial t} = \left(\frac{EA}{2L}\int_0^L \left(\frac{\partial z}{\partial x}\right)^2 \mathrm{dx}\right)\frac{\partial^2 z}{\partial x^2} + HJ. \tag{7.2}$$

The equations governing the electronic subsystem, see Figure ($7.1(a)$), reads:

$$C\dot{V} = I - V/R[z(t,x)], \tag{7.3}$$

$$\mathcal{L}\dot{I} = V_0 - V, \tag{7.4}$$

where, as usual, V is the voltage drop over the capacitor and I the current. Equations (7.2 - 7.4) are solved numerically using a Galerkin reduced-order model, which we truncate at the 6th overtone. Hence, for the mechanical deflection we make the following Ansatz:

$$z(t,x) = \lambda\sum_{n=0}^{6} u_n(t)\phi_n(x/L), \tag{7.5}$$

where L is the length of the nanowire and ϕ_n is the mode shape corresponding to the frequency ω_n. The resistance R is now treated as a functional of the total vertical bending shape $z(t,x)$ and is integrated numerically at each time step. Furthermore we define

$$\alpha_n = \int_0^1 \phi_n(\hat{x})d\hat{x}, \tag{7.6}$$

where we have used the notation $\hat{x} = x/L$. In Table (7.1) are listed the frequencies and parameters α_n for the first few modes with even index for a carbon nanotube. The effect of the Lorentz force on each mode will be proportinal to α_n which is the reason why we only need to take into account those with even

index n. Extending our definitions further, the mode dependent characteristic length is defined as

$$\lambda_n = -\frac{R}{\partial R/\partial u_n}. \tag{7.7}$$

If, as usual, we rely on the sensitivity of the resistance being achieved through electronic doping controlled by a gate electrode, to a first approximation (see Appendix A) the relative magnitude of the characteristic lengths should be

$$\frac{\lambda_n}{\lambda_m} \approx \frac{\alpha_m}{\alpha_n}. \tag{7.8}$$

Since there is no 'unique' characteristic length for the system as a whole we put λ = 1 nm consistently throughout. Finally we introduce the mode dependent coupling parameter

$$\beta_n = \alpha_n \frac{HJL}{K_n \lambda_n}, \tag{7.9}$$

where $K_n = \omega_n^2 K/\omega_0^2$, K being the effective spring constant for the fundamental mode. In total, it could thus be argued that the coupling parameter β_n should decline at a rate given approximately by

$$\beta_n \approx \frac{\alpha_n^2}{\alpha_0^2}\frac{\omega_0^2}{\omega_n^2}\beta_0. \tag{7.10}$$

Recalling from our previous analysis, that (neglecting non-linear forces and intermode crosstalk) when $\beta_n S_n$ is negative the mode becomes unstable approximately when

$$|\beta_n S_n| > 1/Q, \tag{7.11}$$

it is evident that Equation (7.10) puts severe limits on how high frequencies we can actually reach. Therefore, at this point it could be appropriate to say a few words about the maximum current that a carbon nanotube can withstand. In Ref [38] it was reported that for single-walled carbon nanotube with a length of approximately 1μm, at room temperature the current tends to saturate at around 20μA. The current carrying capacity of multi-walled carbon nanotubes

Table 7.1: Mode dependent vibrational frequencies ω_n and integration constants α_n for the first four bending modes with even index of a carbon nanotube.

n	ω_n/ω_0	α_n
0	1	0.83
2	5.4	0.36
4	13.3	0.23
6	24.8	0.17

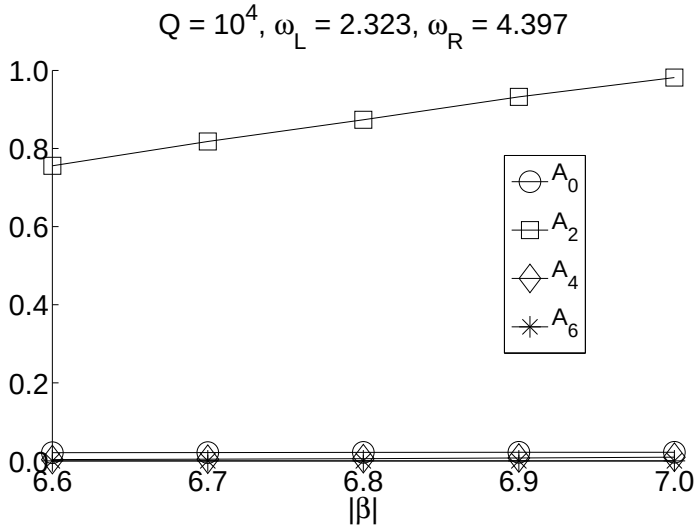

Figure 7.2: Saturation amplitudes A_0, A_2, A_4 and A_6 for the respective modes u_0, u_2, u_4 and u_6, as a result of computer simulations aimed at selective self-excitation of the second harmonic of a carbon nanotube with radius $r = 1$nm and length $L = 1\mu$m.

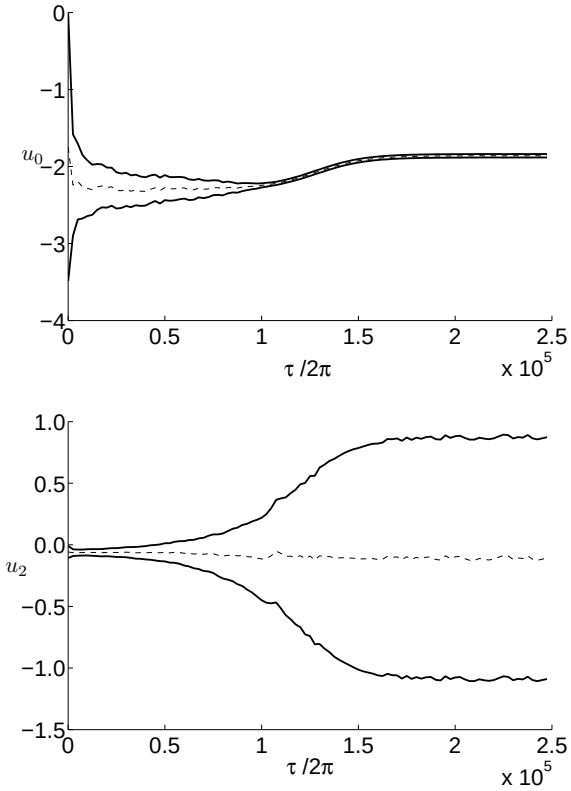

Figure 7.3: Time evolution of the envelopes of the rapid oscillations in the fundamental mode u_0 (top figure) and second harmonic u_2 (bottom figure) of a carbon nanotube as the results of a computer simulation displaying a normal selective excitation.

is higher though [39].

In Figure (7.2) we show the saturation amplitudes for the respective modes as a result of computer simulations for a coupling parameter β in the range -6.6 to -7.1 which, assuming a stationary current of 1 μA, corresponds to a magnetic field strength in the interval 2.6-2.8 T. The quality factor was assumed to be $Q = 10^4$ and the electronic frequencies where chosen so as to selectively excite the second overtone. Figure (7.3) shows the envelopes of the rapid oscillations as a function of time of the zeroth and second mode for one of these simulations. As we can see, in the beginning the fundamental mode oscillates with the largest amplitude but later on the second harmonic experiences a rapid boost which causes the magnitude of the timeaveraged displacement in the fundamental mode to decrease. This is because the oscillation increases the effective resistance leading to a reduced Lorentz force.

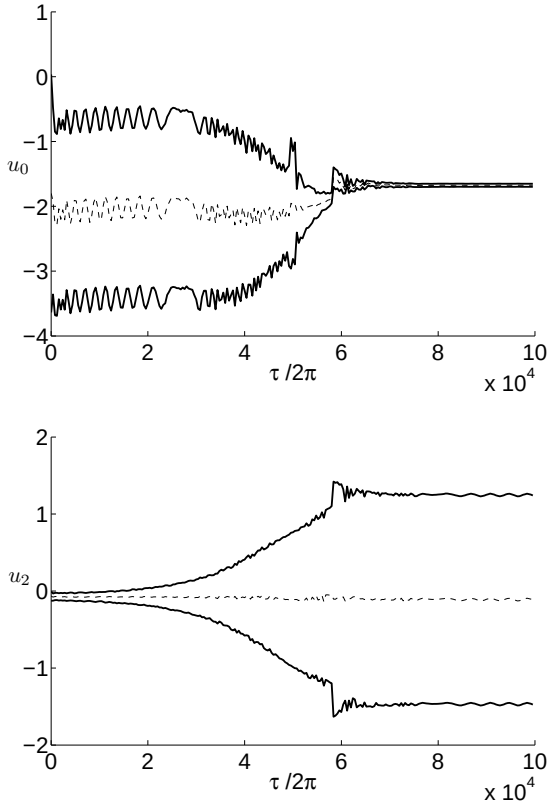

Figure 7.4: Time evolution of the envelopes of the rapid oscillations in the fundamental mode u_0 (top figure) and second harmonic u_2 (bottom figure) of a carbon nanotube as the results of a computer simulation in the transition regime. Initially the frequency of the fundamental mode is renormalized above ω_L which is later restored when the second harmonic grows in amplitude.

As an illustration of how the non-linear forces can lead to a somewhat erratic behaviour, in Figure (7.4) we present the results of a computer simulation with the same parameters as in Figure (7.3) except for a slightly larger coupling parameter. What has happened now is that due to the static deflection, the fundamental frequency has initially been renormalized so that it is suddenly larger than ω_L. As the amplitude for second mode grows, however, the effective resistance increases which leads to a reduced static deflection of the fundamental mode which in turn decreses its frequency so that it is again lower than ω_L. This could in a way be thought of as a transition regime, because if the coupling parameter is pushed higher, beyond a second threshold, the entire system enters a chaotic regime that can not be tracked numerically. For carbon nanotubes, the critical amplitude when this occurs is largely dependent on the radius of the tube, which is typically not very large. For this reason, it is worth to turn our attention now to graphene nano-ribbons.

7.2 Graphene nano-ribbons

We recall from Chapter (2) that the one-dimensional equation of motion of a doubly clamped graphene sheet reads

$$\rho\frac{\partial^2 z(t,x)}{\partial t^2}+\rho\gamma\frac{\partial z(t,x)}{\partial t}-T_0\frac{\partial^2 z(t,x)}{\partial x^2}-T_1\frac{\partial}{\partial x}\left(\frac{\partial z(t,x)}{\partial x}\right)^3=P_z(t,x). \quad (7.12)$$

The important thing to notice is that the nonlinear term is not dependent on the width of the sheet, unlike the carbon nanotube where the radius entered explicitly into the equation. Here, it is instead primarily the length of the nanoribbon that determines the critical amplitude of motion when non-linear forces become dominant. The mode shapes ϕ_n are now given by,

$$\phi_n(x)=\sqrt{2}\sin((n+1)\pi x), \quad (7.13)$$

and if we again define $\alpha_n=\int_0^1\phi_n(x)\mathrm{dx}$ we obtain the set of parameters presented in Table (7.2). As we can see, the α_n decline more rapidly than for

Table 7.2: Mode dependent vibrational frequencies ω_n and integration constants α_n for the first four streching modes with even index of a graphene nano-ribbon.

n	ω_n/ω_0	α_n
0	1	0.90
2	3	0.30
4	5	0.18
6	7	0.13

carbon nanotubes while the frequencies increase at a slower rate. Both these facts would make a graphene nano-ribbon inferior to a carbon nanotube if it hadn't been for the fact that the amplitude range within the linear regime is greater by almost a factor ten already when comparing a graphene nano-ribbon of length 1μm to a nanotube of the same length and with radius 1 nm. This can be further extended for graphene by simply making it longer. Numerical simulations were performed, now with the coupling parameter

$$\beta = \frac{HV_0}{AR_0}\frac{t_0^2}{\lambda\rho}, \tag{7.14}$$

where A is the area of the graphene sheet and $t_0 = L\sqrt{\rho/T_0}$. One might think that a small area is beneficial, but on the other hand a larger sheet has a higher current carrying capacity so these two factors are likely to cancel each other. A graphene nanoribbon of width 10nm, which is comparable to the typical circumference of a carbon nanotube, could be expected to have a current carrying capacity of approximately 100 μ A, see Ref [40]. In Figure (7.5) we show the saturation amplitudes resulting from a number of computer simulations aimed at exciting the second mode. One obvious difference compared with carbon nanotubes is that there is less of a difference between the saturation amplitude of the excited mode and that of the other modes. For graphene they differ typically by a factor 10 whereas for nanotubes it is almost by a factor 100.

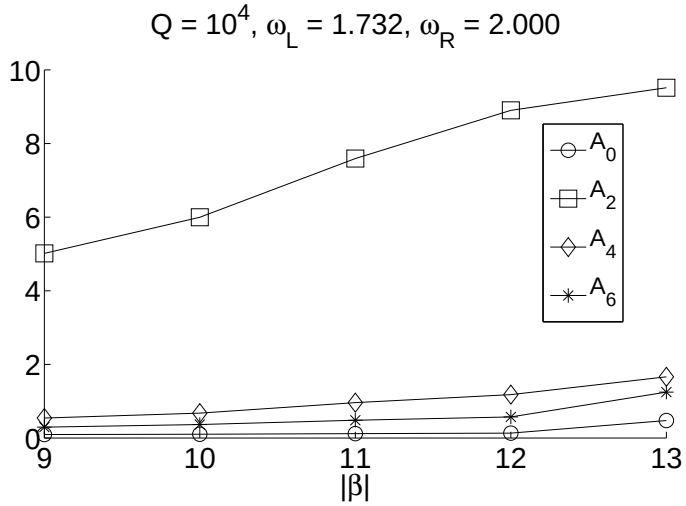

Figure 7.5: Saturation amplitudes A_0, A_2, A_4 and A_6 for the respective modes u_0, u_2, u_4 and u_6, as a result of computer simulations aimed at selective self-excitation of the second harmonic of a graphene nano-ribbon of width $w = 10$nm and length $L = 1\mu$m.

CHAPTER 8

The Transmission Line

We may carry out the same analysis as in Chapter 5 with the magnetic force replaced by an electrostatic force. As mentioned before, in this case the typical geometry would be an STM-tip positioned above the CNT. We may argue that due to some effective capacitance at the junction there will be a charge build-up which in turn results in an electrostatic attraction between the STM-tip and the CNT, see figure (8.1). A first attempt at modelling this kind of system could be to use the same dynamical systems as before but with the Lorentz force replaced by the electrostatic force

$$F_{ext} = \frac{1}{2}\alpha q^2, \tag{8.1}$$

for some constant α, q denoting the charge. What we should remember is that the electrostatic force can only pull in one direction, it cannot be reversed as in the case of a magnetic field. In particular that means that in the current bias regime we can only hope to achieve instability whereas in the voltage bias regime we can obtain both instability and cooling. The resulting formulas are similar to those already derived and are therefore presented in Appendix C. In the following section we will instead focus on another model called the transmission line. The idea behind this model is that due to some internal capacitance and inductance in the wire the charge cannot escape immediately but instead propagates like a wave through a medium with a certain finite velocity. The underlying physical reality that motivates the use of a transmission line model may vary. A common belief is that the elementary electronic excitations of a carbon nanotube behave like a so called Luttinger Liquid. A thorough quantum mechanical treatment of the electronic properties of precisely this kind of system, an STM-tip placed above a carbon nanotube treated as a Luttinger Liquid, was done in the papers [41–43]. Here we will attempt to incorporate mechanics into the consideration and figure out under which conditions this kind of system will exhibit electro-mechanical instability. A full quantum mechanical treatment of this problem will not be provided here, partly because it is too difficult and partly because there is a substantial probability that it would turn out to be redundant in the end. Instead we will jump directly into the transmission line model and draw heavily upon the excellent paper of P. J. Burke [44] for the justification of certain physical parameters.

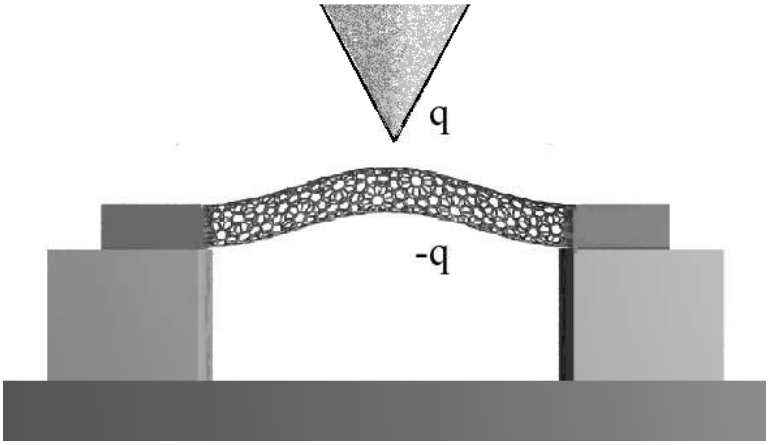

Figure 8.1: Illustration of the electrostatic attraction between an STM-tip and a suspended CNT.

We imagine the nanotube to be composed of a series of segments each with a capacitance C_n and a charge q_n and that there is also some uniform selfinductance $\mathcal{L}$ in the wire. The electronic scheme for this model is shown in Figure (8.2). In this idealized model the transmission line does not have an end but extends without interruption to infinity. Thus, unlike all the previous systems, here we only have one 'contact'. The variables φ_n mark the electrostatic potential at each segment on the line and I_n denotes the current between the potentials φ_n and φ_{n+1}. The capacitance at the contact between the STM-tip and the CNT is denoted C_0 and it is assumed that the entire resistance is concentrated to this point. As usual, the resistance is dependent on the position of the CNT. Furthermore, if we assume that all C_n except for C_0 are equal and independent of u we obtain the following equations:

$$\varphi_{n+1} - \varphi_n = -\mathcal{L}\dot{I}, \tag{8.2}$$

$$q_n = C_n\varphi_n, \tag{8.3}$$

$$\dot{q}_n = \frac{d}{dt}(C_n\varphi_n) = I_{n-1} - I_n + \delta_{n0}(V - \varphi_n)/R(u), \tag{8.4}$$

$$C_n = C + \Delta C(u)\delta_{n0}. \tag{8.5}$$

The difference between the capacitance of the segments and that of the contact is assumed to be dependent on the position of the nanowire and is here given by $\Delta C(u)$. We now introduce the following variables:

$$\chi_n = \int_{-\infty}^{t} \varphi_n(t')dt', \tag{8.6}$$

and the following discrete nabla operators

$$\nabla_- \chi_n = \chi_n - \chi_{n-1}, \tag{8.7}$$

$$\nabla_+ \chi_n = \chi_{n+1} - \chi_n. \tag{8.8}$$

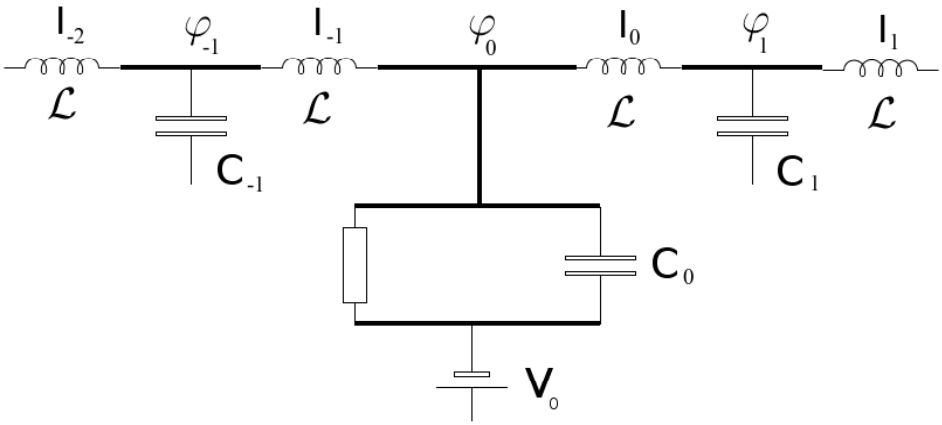

Figure 8.2: Electronic scheme of the transmission line.

Given these definitions we can express the current as

$$I_n = -\frac{1}{\mathcal{L}}\nabla_+\chi_n, \tag{8.9}$$

and hence

$$I_{n-1} - I_n = -\nabla_-(-\frac{1}{\mathcal{L}}\nabla_+\chi_n) = \frac{1}{\mathcal{L}}(\chi_{n+1} - 2\chi_n + \chi_{n-1}). \tag{8.10}$$

The right hand side of the above equation we recognize as the discrete Laplace Operator. Thus, it is natural to go the continuum limit by making the following transitions:

$$\frac{1}{\mathcal{L}}(\chi_{n+1} - 2\chi_n + \chi_{n-1}) \to \frac{1}{\mathcal{L}}\frac{\partial^2\chi}{\partial x^2}, \tag{8.11}$$

$$\delta_{n0} \to \delta(x). \tag{8.12}$$

The careful reader may have noticed that, for convenience, the 'step-length' was circumvented for the Laplace operator, something that we will get back to later. Equation (8.4) is then transformed to

$$(C + \Delta C(u)\delta(x))\frac{\partial^2\chi}{\partial t^2} + \frac{\partial\chi}{\partial t}\Delta C'(u)\dot{u}\delta(x) = \frac{1}{\mathcal{L}}\frac{\partial^2\chi}{\partial x^2} + \delta(x)(V - \frac{\partial\chi}{\partial t})/R(u). \tag{8.13}$$

The mechanical motion is given by

$$m\ddot{u} + \gamma\dot{u} + ku = \frac{1}{2}(V - \dot{\chi}(0))^2\Delta C'(u). \tag{8.14}$$

We now define a 'formal' stationary solution $(u_0, \chi_0(x))$ which is the solution of the above equations which also satisfies the conditions $\ddot{u} \equiv \dot{u} \equiv \ddot{\chi} \equiv \dot{\chi} \equiv 0$,

or equivalently:

$$u_0 = \frac{V^2 \Delta C'(u_0)}{2k}, \tag{8.15}$$

$$-\mathcal{L}\frac{\partial^2 \chi_0(x)}{\partial x^2} = \frac{V}{R(u_0)}\delta(x). \tag{8.16}$$

The physical significance of the function $\chi_0(x)$ is somewhat obscure since it does not give rise to any potential or current. It is nevertheless convenient to make the transitions:

$$\chi \to \chi_0 + \chi, \tag{8.17}$$

$$u \to u_0 + u. \tag{8.18}$$

If we keep only linear terms our system of equations becomes

$$\ddot{\chi} - \frac{1}{\mathcal{L}C}\chi'' + \frac{\Delta C}{C}\ddot{\chi}\delta(x) + \frac{1}{RC}\dot{\chi}\delta(x) = \frac{1}{RC}V\frac{u}{\ell}\delta(x), \tag{8.19}$$

$$m\ddot{u} + \gamma\dot{u} + ku = -V\dot{\chi}(0)\Delta C'(u_0), \tag{8.20}$$

where ℓ is the characteristic length defined in Chapter (3). One way to solve these equations is to first obtain the Green's function $g(t,x)$ satisfying

$$\ddot{g} - \frac{1}{\mathcal{L}C}g'' + \frac{\Delta C}{C}\ddot{g}\delta(x) + \frac{1}{RC}\dot{g}\delta(x) = \delta(x)\delta(t-t'). \tag{8.21}$$

By the use of fourier transform techniques (see appendix D) one can show that the physically admissable solution to equation (8.21) which does also obey causality is given by

$$g(t,0) = \frac{\Theta(t-t')}{\omega_L + \omega_R}(1 - e^{-\frac{C}{\Delta C}(\omega_R+\omega_L)(t-t')}), \tag{8.22}$$

$$\dot{g}(t,0) = \Theta(t-t')\frac{C}{\Delta C}e^{-\frac{C}{\Delta C}(\omega_R+\omega_L)(t-t')}, \tag{8.23}$$

where $\omega_R = 1/RC$, $\omega_L = 1/\sqrt{\mathcal{L}C}$ and $\Theta(t-t')$ is the Heaviside function. From the Green's function we recover $\chi(t,0)$ through

$$\chi(t,0) = \frac{V\omega_R}{\ell}\int g(t-t',0)u(t')dt', \tag{8.24}$$

with the time-derivative given by

$$\dot{\chi}(t,0) = \frac{V\omega_R}{\ell}\int \dot{g}(t-t',0)u(t')dt'. \tag{8.25}$$

Finally we combine equations (8.20) and (8.25) to get the time-evolution of u:

$$m\ddot{u} + \gamma\dot{u} + ku = -\frac{V^2\omega_R\Delta C'(u_0)}{\ell}\int \dot{g}(t-t',0)u(t')dt'. \tag{8.26}$$

If we make the ansatz

$$u(t) = e^{i\omega t}, \tag{8.27}$$

where ω may be any complex number, the integro-differential equation (8.26) reduces to the algebraic equation

$$(-\omega^2 + i\omega\omega_0 Q^{-1} + \omega_0^2)(\frac{C}{\Delta C}(\omega_L + \omega_R) + i\omega) + \frac{V^2 C}{\ell k}\frac{\Delta C'}{\Delta C}\omega_0^2\omega_R = 0, \tag{8.28}$$

where as usual Q is the quality factor and $\omega_0 = \sqrt{k/m}$ is the mechanical frequency. Solutions to equation (8.28) with negative imaginary part correspond to solutions to equation (8.26) for which the amplitude increases in time. The latter would correspond to the instability discussed in previous sections. The condition for unstable solutions turns out to be

$$\frac{V^2 C}{\ell k}\frac{\Delta C'}{\Delta C} > Q^{-1}\frac{\omega_0}{\omega_R} + Q^{-1}\left(\frac{C}{\Delta C}\right)^2\frac{(\omega_L+\omega_R)^2}{\omega_0\omega_R} + Q^{-2}\frac{C}{\Delta C}\frac{\omega_L+\omega_R}{\omega_R}. \tag{8.29}$$

Since the right hand side of the above inequality is always positive, a necessary requirement for self-excitations is that the ratio $\Delta C'/\Delta C$ be positive, something that is likely to be the case for the geometry considered. In order to estimate the parameters involved in the expression above we first return to equation (8.11). Introducing the steplength Δx the correct transition ought to read

$$\frac{1}{\mathcal{L}C}(\chi_{n+1} - 2\chi_n + \chi_{n-1}) = \frac{(\Delta x)^2}{\mathcal{L}C}\frac{\chi_{n+1} - 2\chi_n + \chi_{n-1}}{(\Delta x)^2} \to \frac{(\Delta x)^2}{\mathcal{L}C}\frac{\partial^2\chi}{\partial x^2}. \tag{8.30}$$

Obviously, both the capacitance and inductance depends on the discretization used. In Ref [44], the kinetic inductance per unit length of a carbon nanotube is estimated as

$$\mathcal{L}_K = \frac{h}{2e^2 v_F} \approx 16\,\mathrm{nH}/\mu\mathrm{m}, \tag{8.31}$$

and the quantum capacitance per unit length as

$$\mathcal{C}_Q = \frac{2e^2}{hv_F} \approx 100\,\mathrm{aF}/\mu\mathrm{m}. \tag{8.32}$$

Hence, by putting $\mathcal{L} = \mathcal{L}_K\Delta x$ and $C = \mathcal{C}_Q\Delta x$ we obtain

$$\omega_L = \sqrt{\frac{1}{\mathcal{L}_K\mathcal{C}_Q}} = v_F = 8\cdot 10^5\,\mathrm{s}^{-1}, \tag{8.33}$$

which is in fact rather slow compared with the typical mechanical resonance frequences. From the expression (8.34) it is obvious that this fact promotes instability, in the extreme case of zero inductance there would be no such possibility. Moving on to the mutual capcitance between the nanotube and the STM-tip, a fair estimate [25,45] would be $\Delta C = 1$ aF. It is also reasonable that the two characteristic lengths should be approximately $\ell \sim \Delta C/\Delta C' \sim 1$ nm. Moreover, the resistance is likely to be of the order $R \sim 1$ MΩ. What now remains is the transmission line capacitance C, which obviously depends on the mesh size. There is, however, a possibility to circumvent this parameter completely. As we argued before, the LC-frequency ω_L is entirely independent of the mesh size. Hence, by keeping ω_L constant and letting $\Delta x \to 0$, this is equivalent of taking the limit $C \to 0$ in expression (8.34), which then becomes:

$$\frac{V^2}{\ell k}\frac{\Delta C'}{\Delta C} > Q^{-1}\omega_0 R + Q^{-1}\frac{1}{(\Delta C)^2\omega_0 R} + Q^{-2}\frac{1}{\Delta C}. \tag{8.34}$$

If we assume that $k \sim 10^{-5}$N/m, $\omega_0 = 10^9 s^{-1}$ and $Q = 10^4$ then given our other estimations the critical voltage for instability is roughly

$$V_c \sim 1\mathrm{mV}. \tag{8.35}$$

This is in fact a very modest value, which indicates that the electronic inertia caused by the accumulation of charges inside the nanotube could very well be sufficient to cause instability. However, there remain some questions that could be the material for future research, for example how the instability evolves in time.

CHAPTER 9

Spintromechanics

In the previous chapters the function of the magnetic field has been onefold, its only purpose was to induce a Lorentz force. In what follows we will analyze a system in which the magnetic field in fact plays three roles. Apart from the Lorentz force feedback it is also responsible for splitting the spin degenerate energy levels inside the nanotube and for inducing an electromotive force.

We consider a carbon nanotube suspended between a normal and a spin-polarized lead, see Figure (9.1). There are two features that are crucial for the occurence of the phenomena to be discussed in the following. The most obvious is the spin-polarization in the lead acting as the drain which prohibits electrons with spin up to tunnel from the carbon nanotube into that lead. Full polarization is not a necessary condition, however, but for clarity we present the calculations only for this case. Secondly, we assume the electron-electron repulsion to be so strong that the nanotube can only be populated by one electron at a time. The latter is often referred to as Coulomb blockade. In principle this system can be treated by a full quantum mechanical description, but much effort can be saved by instead describing it through something called rate-equations [46, 47]. If we let P_0 be the probability that the nanotube is unpopulated, $P_{\uparrow(\downarrow)}$ the probability that it is populated by an electron with spin up (down) then, imposing the coulomb blockade constraint, we get the following simple relation

$$P_0 + P_\uparrow + P_\downarrow = 1. \tag{9.1}$$

If we let Γ_S and $\Gamma_D^\downarrow$ denote the tunneling coefficients between the nanotube and the source/drain electrode respectively, (downarrow included to emphasize that only spin-down electrons can tunnel between the nanotube and the drain), we obtain the following rate equations:

$$\begin{aligned} \dot{P}_\uparrow &= \Gamma_S P_0 f_\uparrow(V,H) - \Gamma_S P_\uparrow (1 - f_\uparrow(V,H)) \\ \dot{P}_\downarrow &= \Gamma_S P_0 f_\downarrow(V,H) - \Gamma_S P_\downarrow (1 - f_\downarrow(V,H)) - \Gamma_D^\downarrow P_\downarrow \end{aligned} \tag{9.2}$$

where

$$f_{\uparrow,\downarrow}(V,H) = \left(\exp\left[\tfrac{1}{k_B T} \left(\pm \tfrac{1}{2} \mu_B H - eV \right) \right] + 1 \right)^{-1} \tag{9.3}$$

is the Fermi-function describing the available energy states in the source-lead. In principle one could also introduce the Fermi-function for the drain as well,

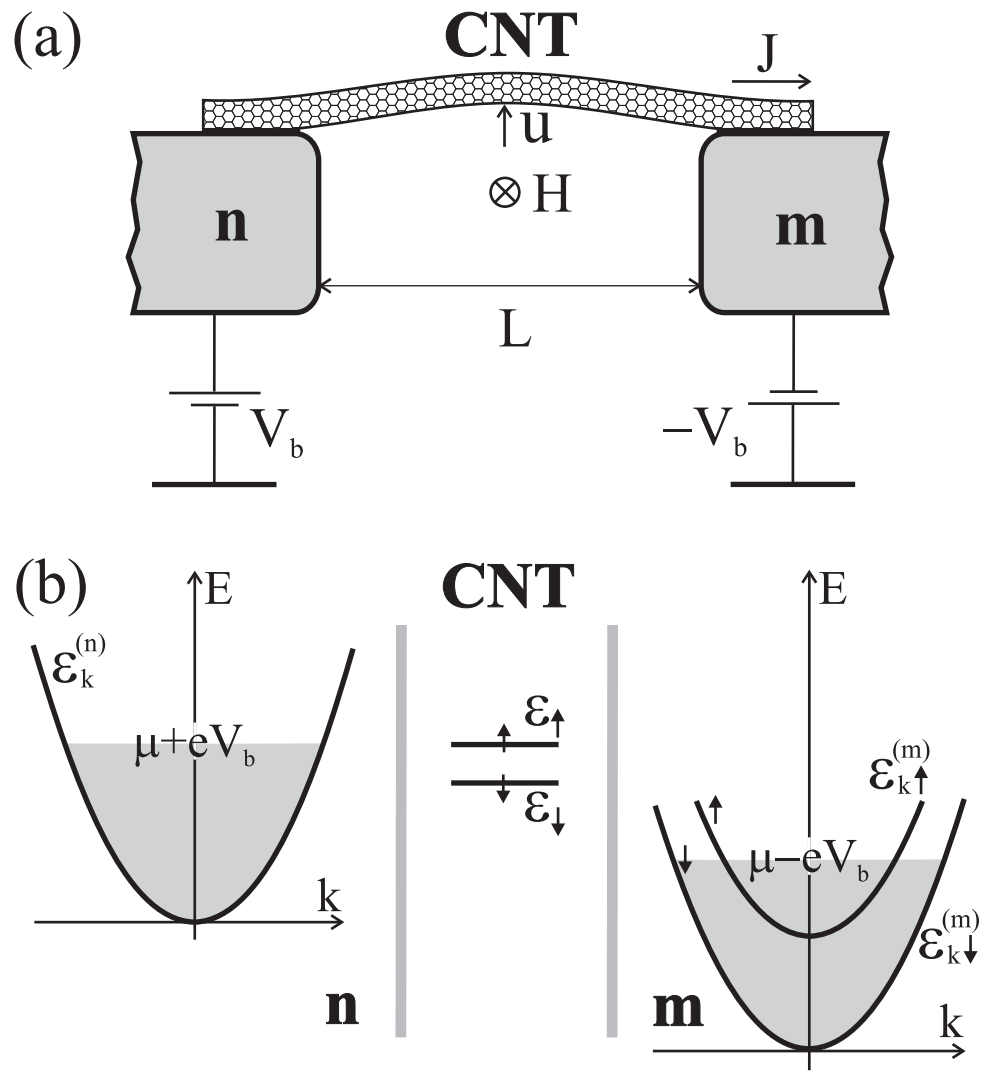

Figure 9.1: (a) A carbon nanotube (CNT) subject to an external magnetic field H, suspended between normal- (n) and magnetic (m) metal leads biased by voltages $\pm V_b$. (b) Electronic energy scheme for the junction: μ is the chemical potential, $\varepsilon_{\uparrow,\downarrow}$ are spin-split levels in the CNT, $\varepsilon_k^{(n)}$ and $\varepsilon_{k\sigma}^{(m)}$ are electron energy bands in the leads (k is the wave vector, σ is spin).

but here we have assumed that the energy gap between the spin down level in the nanotube and the chemical potential in the drain is so large that for the temperatures considered we may just as well put $f_{\uparrow,\downarrow}(V,H) = 0$ for the drain electrode, which means that, first of all, there will always be an available state in the drain for the spin-down electron to occupy and, secondly, there is no possibility for electrons to tunnel from the drain into the nanotube. The net current is given by the expression

$$J(V,H) = e\Gamma_D^{\downarrow} P_{\downarrow}^{(0)}(V,H) \tag{9.4}$$

where $P_{\downarrow}^{(0)}(V,H)$ is the stationary probability to find a spin-down electron in the nanotube, obtained as the time independent solution of the equations (9.2). Given this solution the current can be expressed as:

$$J(V,H) = e\Gamma_D^{\downarrow} \frac{f_{\downarrow}(V,H)(1 - f_{\uparrow}(V,H))}{1 + \Gamma_D^{\downarrow}/\Gamma_S - f_{\uparrow}(V,H) f_{\downarrow}(V,H)}. \tag{9.5}$$

Using a so called 'quasi-static' approximation, which roughly means that the mechanics is so slow in comparison with the electronics that retardation effects can be neglected, the dynamics of the fundamental mode of the nanotube is given by

$$m\ddot{u} + \tilde{\gamma}\dot{u} + \omega_0^2 u = \alpha H L J(V_b - \alpha H L \dot{u})\,. \tag{9.6}$$

The right hand side is simply the Lorentz force, but where the current is affected by the electromotive force induced by the vertical motion of the nanotube. The parameter α, occurring twice in the equation, is simply a geometrical shape factor corresponding to the particular bending mode. The criterion for instability of this system turns out to be

$$\beta \equiv -\frac{\alpha^2 H^2 L^2}{m} J'(V_b) - \frac{\omega}{Q} > 0\,. \tag{9.7}$$

where $J'(V) = dJ(V)/dV$ is simply the current-voltage characteristic. Evidently, in the 'quasi-static' case instability can only occur for a negative differential resistance, unlike most of the previous systems considered in this thesis. The system at hand does however exhibit some interesting features that were not present before. Assuming that the mechanical motion has the form $u(t) = u_0 + A(t)\cos(\omega t)$, where the amplitude A varies slowly on the timescale of the rapid oscillations, and inserting it into Equation (9.6) we obtain:

$$\begin{aligned} &\dot{A} = -\Phi(A); \\ &\Phi(A) = \frac{\omega A}{2Q} \quad + \quad \frac{\alpha H L}{m\omega} \int_{-\pi}^{\pi} \frac{d\phi}{2\pi} J(V_b + \alpha H L \omega A \sin\phi) \sin\phi. \end{aligned} \tag{9.8}$$

The behaviour of the function Φ for some parameter values is shown in Figure (9.2). In the figure to the left we see an example of emergence of soft instability

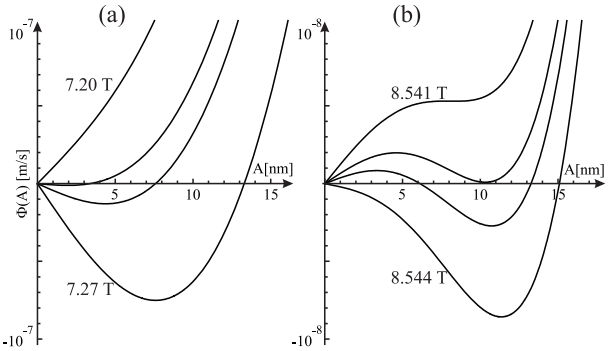

Figure 9.2: Behaviour of the function $\Phi(A)$ defined in Eq. (9.8) for different magnetic fields leading to (a) soft excitation of nanowire oscillations at $\Delta V \equiv V_b - (\epsilon_0 - \mu)/e = 0.34$ mV and (b) hard excitation at $\Delta V = 0.41$ mV. Other parameter values are $T = 0.2$ K, $Q = 3 \cdot 10^4$, $\Gamma_D^{\downarrow}/\Gamma_S = 0.4$, $\omega/\Gamma_S = 0.2$

and in the figure to the right we see an example of hard instability. Moreover, in the rightmost figure we can see that before the onset of hard instability there is an intermediate region where if the nanotube is given a suffiently large initial amplitude the system will not bring it back to zero but instead take it to a stationary state of oscillation marked by the second crossing of the horizontal line. This intermediate region we call the region of bistability.

In the systems considered in previous chapters, the stationary oscillations were also associated with a deviation in the time averaged current. This deviation was almost always a reduction, only in exotic situations could you expect an increase. The system at hand is one of these exotic cases. The formula for the time averaged current is given by

$$\bar{J} = \int J(V_b + \alpha H L \omega A \sin\phi) d\phi / 2\pi. \tag{9.9}$$

In Figure (9.3) we merge all the phenomena discussed here into one piece. In the upper figure we have the regions of stability, bistability and instability plotted in a diagram showing the voltage versus magnetic field. In the figures below is shown the average current as we sweep the voltage or magnetic field over a region passing from stability over to bistability and instability. As is evident, in the case of hard instability we may obtain a hysteretic behaviour in the time-averaged current while passing through the bistability region which, if verified experimentally, would constitute a convincing 'fingerprint' of the phenomena theoretically derived.

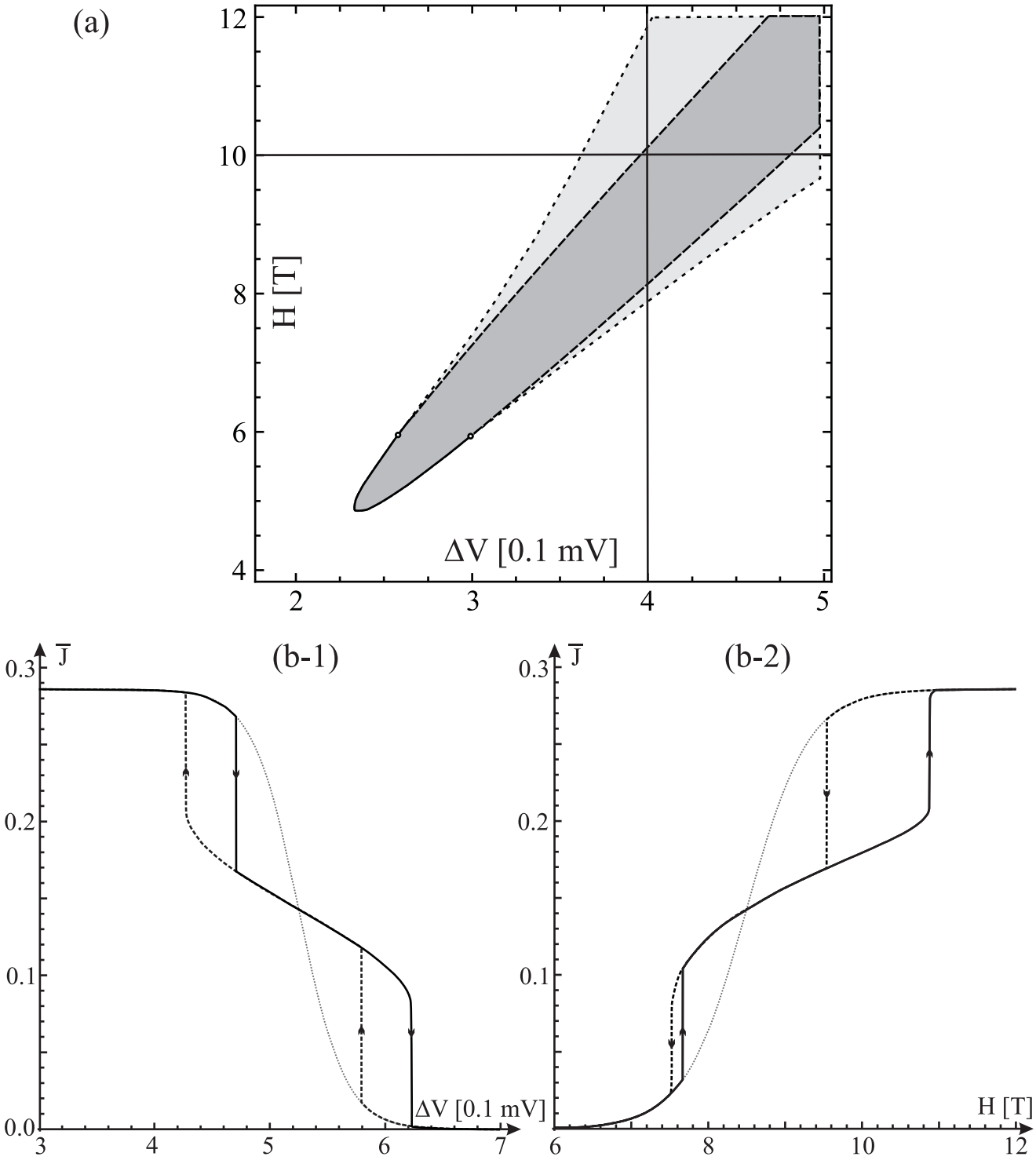

Figure 9.3: (a) Stability diagram for nanowire oscillations in the $(H, \Delta V)$ plane, where $\Delta V = V_b - (\epsilon_0 - \mu)/e$. In the white and dark grey regions there is only one stable stationary state corresponding to a non-moving and a vibrating nanowire, respectively. The light gray region is where both these states are stable. (b) Average current in units of $e\Gamma_S$, in (b-1) as a function of bias voltage ΔV for $H = 10$ T [horizontal line in (a)] and in (b-2) as a function of magnetic field H for $\Delta V = 0.4$ mV [vertical line in (a)]. The full (dashed) lines show the result for an ascending (descending) magnetic field. The gray dotted curves correspond to a static nanowire. Other parameters: $T = 0.2$ K, $Q = 3 \cdot 10^4$, $\Gamma_D^{\downarrow}/\Gamma_S = 0.4$, $\omega/\Gamma_S = 0.1$.

CHAPTER 10

Concluding Remarks

To summarize, in this thesis we have explored a number of NEMS devices with the common feature that they are all capable of producing mechanical self oscillations. Some of these emerge as a result of a negative differential resistance but in most cases this is not required. Most of them result in a drop in average current, but there is at least one exception from this rule. Some are mathematically relatively simple while others are more complicated, but as we have seen, simplicity does not stand in opposition to versatility. On the contrary, even the simplest device demonstrates the entire range of functionality, all the way from cooling up to an S-shaped I-V characteristic.

A question that poses itself in light of these results is if there is a more general framework in which all different instances of electro-mechanical instability fit in. Knowlege of such a general theory could perhaps provide a tool to tailor the system geomtery so that it, for example, meets the requirements of a certain application and not merely come out as a 'lucky shot'. But this belongs to future research.

Appendix A: Characteristic length of Electronic Doping

In this section we estimate the characteristic length for a semiconducting carbon nanotube suspended over a gate electrode, following closely the derivation of Zhou et al. [18]. Considering first a semiconducting single walled carbon nanotube, the dispersion relation ressembles that of relativistic one-dimensional fermions:

$$E = \pm\sqrt{(m^* v_0^2)^2 + (\hbar k v_0)^2}, \tag{10.1}$$

$$v = \frac{1}{\hbar}\frac{dE}{dk} = \frac{\hbar v_0^2 k}{E}. \tag{10.2}$$

Here, v_0 is the fermi velocity of graphene and the effective mass m^* depends on the tube diameter d and the fermi velocity v_0 through the expression $m^* = 2\hbar/3dv_0$. For the conductance we employ a Drude model for a one-dimensional conductor with four channels:

$$G = \frac{4e^2}{h}\frac{\tau_F v_F}{L} = \frac{4e^2}{h}\frac{l_F}{L}. \tag{10.3}$$

In the formula above v_F is the fermi velocity of the carbon nanotube and τ_F is the scattering time. The constant $G_0 = 2e^2/h$ is often referred to as the conductance quantum. Furthermore, in one dimension the fermi momentum k_F is related to the carrier concentration n through the expression:

$$k_F = \frac{\pi n}{4}. \tag{10.4}$$

Hence, according to our model, the carrier concentration affects the conductance by shifting the fermi velocity. In turn, the carrier concentration depends on the gate voltage V_g and gate capacitance per unit length C_g' according to:

$$n = \frac{C_g'(V_g - \varphi)}{e}, \tag{10.5}$$

where φ is the potential on the nanotube. In summary, after a few manipulations we obtain the following formula for the resistance per unit length $\rho(n) = 1/G(n)$:

$$\rho(n) = \frac{h}{4e^2 l_F}\frac{1 + (\frac{3\pi}{4}nr)^2}{(\frac{3\pi}{4}nr)^2}. \tag{10.6}$$

Here r is the radius of the tube and $l_F = v_F \tau_F$ is the mean free path at the fermi level. Hence, the total resistance is given by

$$R = \int_0^L \rho(n(x))\mathrm{d}x. \tag{10.7}$$

For $r \ll h(x)$, where $h(x)$ is the distance to the gate, we may use the following formula for the gate capacitance per unit length:

$$C_g'(x) = \frac{2\pi\epsilon_0}{\ln(2h(x)/r)}. \tag{10.8}$$

Calculating the total resistance from $(10.5 - 10.8)$ is quite a complicated task, especially if one takes into account that the potential φ is also a function of carrier concentration [20]. If we consider the situation with a straight wire ($h(x) \equiv h_0$), and for simplicity assume that the potential φ is uniform, if we taylor expand (10.6) and (10.8) to first order and take the limit $V_g \to \varphi$ we obtain the minimal characteristic length

$$(\ell_R)_{min} = \alpha \frac{h_0 \ln(\frac{2h_0}{r})}{2}, \tag{10.9}$$

where $\alpha = L/\int_0^L u_0 \mathrm{d}x$ is just a shape factor. If, for example, we take $h_0 = 50\mathrm{nm}$ we obtain a characteristic length in the order of $10^{-7}\mathrm{m}$, therefore we estimate the minimal characteristic length to lie somewhere between $10^{-7}\mathrm{m}$ and $10^{-6}\mathrm{m}$.

Appendix B: Linear Stability Analysis

Consider the dynamical system

$$\begin{aligned}\dot{x} &= f(x, y, z, ...)\\ \dot{y} &= g(x, y, z, ...)\\ \dot{z} &= h(x, y, z, ...)\\ &....\end{aligned}$$

and let $(x_0, y_0, z_0, ...)$ be a stationary solution. The characteristic polynomial $P(\lambda)$ of the stationary solution is defined as

$$P(\lambda) = \begin{vmatrix} f'_x - \lambda & f'_y & f'_z & \dots \\ g'_x & g'_y - \lambda & g'_z & \dots \\ h'_x & h'_y & h'_z - \lambda & \dots \\ \dots & \dots & \dots & \dots \end{vmatrix},$$

where the derivatives are evaluated at the stationary point. If there are solutions to the equation

$$P(\lambda) = 0 \tag{10.10}$$

with positive real part then small perturbations from the stationary point will increase in magnitude. This is the mathematical notion of instability. There are a number of techniques to determine weather there are such solutions without actually solving the equation. For dimensions less than five a good method is the so called argument principle from complex analysis.

Appendix C: Instability and Cooling through an Electrostatic Force

Here we will discuss the systems analyzed in Chapters (5) and (6) but with the difference that the Lorentz force is replaced by an electrostatic force between the nanotube and an STM-tip placed in its vicinity, see figure (10.1). For previous work on similar problems see for example [6, 27]. Furthermore we assume that the tunneling current increases with decreasing distance. Obviously, in this case we have a situation where the characteristic length is always positive, so in order to achieve some variability in terms of excitation and cooling we need to be in the voltage bias regime. Hence, for brevity, we will only consider this case.

The equations governing this system read

$$m\ddot{u} + \gamma\dot{u} + ku = \frac{1}{2}\alpha q^2, \tag{10.11}$$

$$\dot{q} = I - V/R(u), \tag{10.12}$$

$$\mathcal{L}\dot{I} = V_0 - q/C. \tag{10.13}$$

Introducing the dimensionless current $\psi = I/I_0$, with $I_0 = V_0/R(u_0)$, we have the equivalent system

$$\ddot{\beta} + Q^{-1}\dot{\beta} + \beta = \beta_0\varphi^2, \tag{10.14}$$

$$\dot{\varphi} = \frac{\omega_R}{\omega_0}(\psi - \varphi f(\beta)), \tag{10.15}$$

$$\dot{\psi} = \frac{\omega_L^2}{\omega_R\omega_0}(1 - \varphi), \tag{10.16}$$

where

$$\beta_0 = \frac{\alpha C^2 V_0^2}{2k\ell(u_0)}. \tag{10.17}$$

The exact condition for instability reads

$$\frac{1}{2}(1+\frac{1}{Q}\frac{\omega_R}{\omega_0}+\frac{\omega_L^2}{\omega_0^2})+\sqrt{\frac{1}{4}(1+\frac{1}{Q}\frac{\omega_R}{\omega_0}+\frac{\omega_L^2}{\omega_0^2})^2-\frac{\omega_L^2}{\omega_0^2}} < \frac{(\omega_R/\omega_0)(1+\omega_L^2/(\omega_R\omega_0 Q)+2\beta_0)}{\omega_R/\omega_0+1/Q}. \tag{10.18}$$

In order to determine whether we may under certain circumstances achieve cooling, and in that case at what efficiency, the method outlined in Chapter (6) will not work, or at least there is no obvious way to extract the correct answer from it. The reason for this is the qudratic force term, or more specifically the fact that

$$\int_0^{2\pi} (a\cos(t) + b\sin(t))^2 \cos(t)\mathrm{dt} = 0 \tag{10.19}$$

for all constants a and b. The method thus falsely indicates that we would have a null result to first order in amplitude. The correct result is instead obtained from a perturbation analysis of the characteristic equation. If we consider first the equation for the harmonic oscillator without coupling term

$$\ddot{\beta} + Q^{-1}\dot{\beta} + \beta = 0, \tag{10.20}$$

the solutions to the corresponding characteristic equation $z^2 + Q^{-1}z + 1 = 0$ are given by

$$z = -Q^{-1}/2 \pm \sqrt{Q^{-2}/4 - 1}. \tag{10.21}$$

If we let $P(z)$ be the characteristic polynomial of the coupled system of equations and treat β_0 as a small parameter we can assume that the 'perturbed' solutions $\tilde{z}$ satisfying $P(\tilde{z}) = 0$ can be expressed as

$$\tilde{z} = z + \beta_0 P_1 + \beta_0^2 P_2 + ... \tag{10.22}$$

We now postulate that the succeptibility function is simply $S = \Re P_1$ which in our case yields

$$S = 2\frac{\omega_0\omega_R(\omega_L^2/\omega_0^2 - 1)}{\omega_0^2(\omega_L^2/\omega_0^2 - 1)^2 + \omega_R^2}. \tag{10.23}$$

This is the same function we encountered before except for an extra factor 2. The effect of the electrostatic attraction is thus twice as efficient (expressed in terms of β_0) as the Lorentz force feeback, something that can also be verified by computer simulations. However, there are several ways to argue why the magnetomotive regime could be considered more reliable. One complication with the electrostatic feedback is that when the nanotube moves the mutual capacitance between the nanotube and the STM-tip is likely to fluctuate, something that our model does not take into consideration.

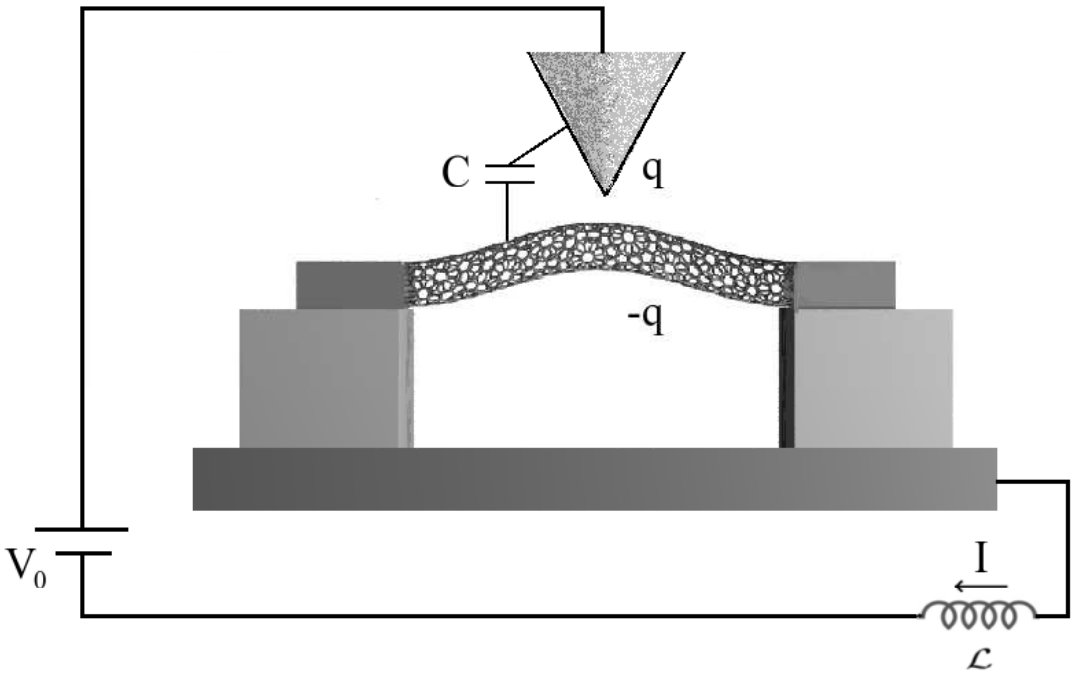

Figure 10.1: The figure shows an electric circuit kept under a constant voltage drop containing an STM-tip positioned above a suspended carbon nanotube. Due to the mutual capacitance between the STM-tip and the CNT, the charge buildup leads to a feedback mechanism is the form of an electrostatic attraction.

Appendix D: Green's Function for the Transmission Line

We wish to solve the equation

$$\ddot{g} - \frac{1}{\mathcal{L}C}g'' + \frac{\Delta C}{C}\ddot{g}\delta(x) + \frac{1}{RC}\dot{g}\delta(x) = \delta(x)\delta(t-t'). \tag{10.24}$$

Let us first introduce the two fourier transforms

$$\hat{f}(\kappa) = \int f(x)e^{-i\kappa x}\mathrm{d}x, \tag{10.25}$$

$$\tilde{f}(\omega) = \int f(t)e^{-i\omega t}\mathrm{d}t, \tag{10.26}$$

with the inverse transforms

$$f(x) = \frac{1}{2\pi}\int \hat{f}(\kappa)e^{-i\kappa x}\mathrm{d}\kappa, \tag{10.27}$$

$$f(t) = \frac{1}{2\pi}\int \tilde{f}(\omega)e^{-i\omega t}\mathrm{d}\omega. \tag{10.28}$$

We know that the action of a fourier transform $\mathcal{F}$ on derivatives follow the rule

$$\mathcal{F}(f'(x))(\kappa) = i\kappa\mathcal{F}(f(x))(\kappa), \tag{10.29}$$

thus equation (10.24) has the following equivalent in fourier space:

$$-\omega^2\tilde{\hat{g}} + \frac{\kappa^2}{\mathcal{L}C}\tilde{\hat{g}} - \omega^2\frac{\Delta C}{C}\tilde{g}(0) + \frac{i\omega}{RC}\tilde{g}(0) = e^{-i\omega t'}, \tag{10.30}$$

which can be rewritten as

$$\tilde{\hat{g}} = \frac{1}{\kappa^2 - \omega^2/\omega_L^2}(e^{-i\omega t'} + (\omega^2\frac{\Delta C}{C} - i\omega\omega_R)\tilde{g}(0))\frac{1}{\omega_L^2}. \tag{10.31}$$

Moreover, we have the identity

$$\tilde{g}(0) = \frac{1}{2\pi}\int \tilde{\hat{g}}\mathrm{d}\kappa. \tag{10.32}$$

When integrating equation (10.31) one must decide over which branch in the complex plane to perform the integral. This will determine the sign of the resulting expression. We will use the following convention:

$$\frac{1}{2\pi}\int \frac{1}{\kappa^2-\omega/\omega_L^2}\mathrm{d}\kappa = \lim_{\delta\to 0}\frac{1}{2\pi}\int \frac{1}{\kappa^2-\omega/\omega_L^2+i\delta}\mathrm{d}\kappa = \frac{1}{2\pi}2\pi i\mathrm{Res}[\kappa=-\omega/\omega_L] = -\frac{i\omega_L}{\omega}, \tag{10.33}$$

whereby we obtain

$$\tilde{g}(0) = -\frac{e^{-i\omega t'}}{\frac{\Delta C}{C}\omega^2 - i\omega(\omega_L+\omega_R)}. \tag{10.34}$$

We may now recover the Green's function by calculating the integral

$$g(t,0) = \frac{1}{2\pi}\int \tilde{g}(0)e^{i\omega t}\mathrm{d}\omega. \tag{10.35}$$

We identify two poles: $\omega = 0$ and $\omega = i\frac{C/\Delta C}{\omega_L+\omega_R}$ with residues $-i/(\omega_L+\omega_R)$ and $i/(\omega_L+\omega_R)e^{-C/\Delta C(\omega_R+\omega_L)(t-t')}$ respectively. For $t-t'>0$ we can close the contour in the upper half plane yielding finally

$$g(t,0) = \frac{\Theta(t-t')}{\omega_L+\omega_R}(1-e^{-C/\Delta C(\omega_R+\omega_L)(t-t')}). \tag{10.36}$$

BIBLIOGRAPHY

[1] K. S. Novoselov, A. K. Geim, S. V. Morozov, D. Jiang, Y. Zhang, S. V. Dubonos, I. V. Grigorieva, and A. A. Firsov, "*Electric Field Effect in Atomically Thin Carbon Films*", Science **306**, 666–669 (2004).

[2] S. Iijima, "*Helical microtubules of graphitic carbon*", Nature **354**, 56–58 (1991).

[3] J. Weldon, B. Alemn, A. Sussman, W. Gannett, and A. Zettl, "*Sustained Mechanical Self-Oscillations in Carbon Nanotubes*", Nano Letters **10**, 1728–1733 (2010).

[4] A. Ayari, P. Vincent, S. Perisanu, M. Choueib, V. Gouttenoire, M. Bechelany, D. Cornu, and S. T. Purcell, "*Self-Oscillations in Field Emission Nanowire Mechanical Resonators*", Nano Letters **7**, 2252–2257 (2007).

[5] V. I. Kleshch, A. N. Obraztsov, and E. D. Obraztsova, "*Electromechanical self-oscillations of carbon nanotube field emitter*", ScienceDirect **48**, 3895–3900 (2010).

[6] L. M. Jonsson, L. Gorelik, R. I. Shekhter, and M. Jonson, "*Electromechanical Instability in Suspended Carbon Nanotubes*", Nano Letters **5**, 1165–1169 (2005).

[7] A. H. C. Neto, F. Guinea, N. M. R. Peres, K. S. Novoselov, and A. K. Geim, "*The electronic properties of graphene*", Reviews of Modern Physics **81**, 109–162 (2009).

[8] J. Charlier, X. Blase, and S. Roche, "*Electronic and transport properties of nanotubes*", Reviews of Modern Physics **79**, 677–732 (2007).

[9] T. Rocheleau, T. Ndukum, C. Macklin, J. B. Hertzberg, A. A. Clerk, and K. C. Schwab, "*Preparation and detection of a mechanical resonator near the ground state of motion*", Nature **463** (2010).

[10] A. Huttel, G. Steele, B. Witkamp, M. Poot, L. P. Kouwenhoven, and H. S. J. van der Zant, "*Carbon Nanotubes as Ultrahigh Quality Factor Mechanical Resonators*", Nano Letters **9**, 2547–2552 (2009).

[11] H. M. Ouakad and M. I. Younis, "*Nonlinear dynamics of electrically actuated carbon nanotube resonator*", Journal of Computational and Nonlinear Dynamics **5**, 011009–1 (2010).

[12] M.-F. Yu, "*Fundamental mechanical properties of carbon nanotubes: Current understanding and the related experimental studies*", Journal of Engineering Materials and Technology **126**, 271–278 (2004).

[13] J. Atalaya, *Theory and Applications of the Mechanics of Graphene Sheets*. PhD thesis, Chalmers University of Technology, 2010.

[14] J. Atalaya, A. Isacsson, and J. Kinaret, "*Continuum Elastic Modeling of Graphene Resonators*", Nano Letters **8**, 4196–4200 (2008).

[15] E. D. Minot, Y. Yaish, V. Sazonova, J.-Y. Park, M. Brink, and P. L. McEuen, "*Tuning Carbon Nanotube Band Gaps with Strain*", PRL **90** (2003).

[16] J. Cao, Q. Wang, and H. Dai, "*Electromechanical Properties of Metallic, Quasimetallic and Semiconducting Carbon Nanotubes under Stretching*", PRL **90** (2003).

[17] C. Stampfer, A. Jungen, R. Linderman, D. Obergfell, S. Roth, and C. Hierold, "*Nano-Electromechanical Displacement Sensing Based on Single-Walled Carbon Nanotubes*", Nano Letters **6**, 1449–1453 (2006).

[18] X. Zhou, J. Park, S. Huang, J. Liu, and P. L. McEuen, "*Band Structure, Phonon Scattering, and the Performance Limit of Single-Walled Carbon Nanotube Transistors*", PRL **95** (2005).

[19] Y. Tarakanov and J. Kinaret, "*A Carbon Nanotube Field Effect Transistor with a Suspended Nanotube Gate*", Nano Letters **7**, 2291–2294 (2007).

[20] Y. Tarakanov, *Carbon-Nanotube-Based Nanoelectromechanical Transistors*. Chalmers University of Technology, 2011.

[21] V. Sazonova, Y. Yaish, H. Ustunel, D. Roundy, T. A. Arias, and P. L. McEuen, "*A tunable carbon nanotube electromechanical oscillator*", Nature **431** (2004).

[22] B. Witkamp, M. Poot, and H. van der Zant, "*Bending-mode vibration of a suspended nanotube resonator*", Nano Letters **6**, 2904–2908 (2006).

[23] B. Lassagne, D. Garcia-Sanchez, and A. Aguasca, "*Ultrasensitive Mass Sensing with a Nanotube Electromechanical Resonator*", Nano Letters **8**, 3735–3738 (2008).

[24] A. A. Shylau, J. W. Klos, and I. V. Zozoulenko, "*Capacitance of graphene nanoribbons*", PRB **80**, 205402 (2009).

[25] B. J. LeRoy, S. G. Lemay, J. Kong, and C. Dekker, "*Electrical generation and absorption of phonons in carbon nanotubes*", Nature **432**, 371–374 (2004).

[26] L. M. Jonsson, F. Santandrea, L. Y. Gorelik, R. I. Shekhter, and M. Jonson, "*Self-organization of irregular nanoelectromechanical vibrations in multimode shuttle structures*", PRL **100**, 186802 (2008).

[27] F. Santandrea, "*Selective Excitations of Transverse Vibrational Modes of a Carbon Nanotube through a "Shuttle-Like" Electromechanical Instability*", Physics Research International (2010).

[28] A. H. Nayfeh, *Introduction to Perturbation Techniques*. Wiley, New York, 1993.

[29] A. Nordenfelt, Y. Tarakanov, L. Y. Gorelik, R. I. Shekhter, and M. Jonson, "*Magnetomotive Instability and Generation of Mechanical Vibrations in Suspended Semiconducting Carbon Nanotubes*", New Journal of Physics **12**, 123013 (2010).

[30] S. Perisanu, A. Ayari, S. Purcell, and P. Vincent, "*Electro-mechanics of Resonating Nanotubes and Nanowires in the Field Emission Environment*", Int. J. of Nanotechnology **7** (2010).

[31] Y.-D. Wang, K. Semba, and H. Yamaguchi, "*Cooling of a micro-mechanical resonator by the back-action of Lorentz force*", New Journal of Physics **10**, 043015 (2008).

[32] K. Jaehne, K. Hammerer, and M. Wallquist, "*Ground-state cooling of a nanomechanical resonator via a Cooper-pair box qubit*", New Journal of Physics **10**, 095019 (2008).

[33] G. Sonne, M. E. Pena-Aza, L. Y. Gorelik, R. I. Shekhter, and M. Jonson, "*Cooling of a Suspended Nanowire by an ac Josephson Current Flow*", PRL **104**, 226802 (2010).

[34] G. Sonne, M. E. Pena-Aza, L. Y. Gorelik, R. I. Shekhter, and M. Jonson, "*Voltage-driven superconducting weak link as a refrigerator for cooling of nanomechanical vibrations*", Low Temperature Physics **36**, 1128–1137 (2010).

[35] A. Nordenfelt, "*Magnetomotive Cooling and Excitation of Carbon Nanotube Oscillations under Voltage Bias*", Central European Journal of Physics **9**, 1288–1293 (2011).

[36] D. Ramos, J. Mertens, M. Calleja, and J. Tamayo, "*Photothermal self-excitation of nanomechanical resonators in liquids*", Appl. Phys. Lett. **92**, 173108 (2008).

[37] H. Fu, C. Liu, Y. Liu, J. Chu, and G. Cao, "*Selective photothermal self-excitation of mechanical modes of a micro-cantilever for force microscopy*", Appl. Phys. Lett. **99**, 173501 (2011).

[38] A. Javey, J. Guo, and M. P. and, "*High-Field Quasiballistic Transport in Short Carbon Nanotubes*", Phys. Rev. Lett. **92**, 106804 (2004).

[39] S. Moon, W. Song, and N. K. and, "*Current-carrying capacity of double-wall carbon nanotubes*", Nanotechnology **18**, 235201 (2007).

[40] R. Murali, Y. Yang, K. Brenner, T. Beck, and J. D. Meindl, "*Breakdown current density of graphene nanoribbons*", Appl. Phys. Lett. **94**, 243114 (2009).

[41] S. Pugnetti, F. Dolcini, D. Bercioux, and H. Grabert, "*Electron tunneling into a quantum wire in the Fabry-Pérot regime*", Physical Review B **79**, 035121 (2009).

[42] M. Guigou, T. Martin, and A. Crépieux, "*Screening of a Luttinger liquid wire by a scanning tunneling microscope tip. I. Spectral properties*", Physical Review B **80**, 045420 (2009).

[43] M. Guigou, T. Martin, and A. Crépieux, "*Screening of a Luttinger liquid wire by a scanning tunneling microscope tip. II. Transport properties*", Physical Review B **80**, 045421 (2009).

[44] P. J. Burke, "*Luttinger liquid theory as a model of the gigahertz electrical properties of carbon nanotubes*", IEEE Transaction on Nanotechnology **1**, 129–144 (2002).

[45] F. Santandrea, L. Y. Gorelik, R. I. Shekhter, and M. Jonson, "*Cooling of Nanomechanical Resonators by Thermally Activated Single-Electron Transport*", Physical Review Lett. **106**, 186803 (2011).

[46] D. Radic, A. M. Kadigrobov, L. Y. Gorelik, R. I. Shekhter, and M. Jonson, "*Self-excited oscillations of charge-spin accumulation due to single-electron tunneling*", Physical Review B **82**, 1098–0121 (2010).

[47] D. Radic, A. Nordenfelt, A. M. Kadigrobov, L. Y. Gorelik, R. I. Shekhter, and M. Jonson, "*Spin-controlled nanomechanics induced by single-electron tunneling*", Physical Review Lett. **107**, 236802 (2011).